Cancer cells retrace a stepwise differentiation program during malignant progression

Sadegh Saghafinia [1,2,3,#], Krisztian Homicsko [1], Annunziata Di Domenico [4], Stephan Wullschleger [1,+], Aurel Perren [4], Ilaria Marinoni [4], Giovanni Ciriello [2,3], Iacovos P. Michael [1,$,#,*], and Douglas Hanahan [1,5,*]

[1] Swiss Institute for Experimental Cancer Research (ISREC), School of Life Sciences, École Polytechnique Fédérale de Lausanne (EPFL), Lausanne, Switzerland

[2] Department of Computational Biology, University of Lausanne (UNIL), Lausanne, Switzerland

[3] Swiss Institute of Bioinformatics (SIB)

[4] Institute of Pathology, University of Bern, Bern, Switzerland

[5] Lausanne Branch, Ludwig Institute for Cancer Research, Lausanne, Switzerland

[+] Current address: Molecular Partners AG, Zurich, Switzerland

[$] Current address: Biological Sciences, Sunnybrook Research Institute, Toronto, Ontario, Canada

[#] These authors contributed equally

[*] Corresponding authors: iacovosm@gmail.com, douglas.hanahan@epfl.ch

Running Title

Retracing stepwise differentiation during tumor progression

Keywords

Pancreatic Neuroendocrine tumor, Dedifferentiation, Cancer plasticity, Tumor heterogeneity, Metastasis, miRNA-181, Hmgb3, Meis2

Corresponding Authors contact details:

Iacovos P. Michael, Sunnybrook Research Institute, 2075 Bayview Avenue, Toronto, Ontario, M4N 3M5, Canada | Phone: 416-480-6100x3354 | E-mail: iacovosm@gmail.com

Douglas Hanahan, ISREC, EPFL, Lausanne, CH-1015, Switzerland | Phone: 41-21-693-0657 | E-mail: douglas.hanahan@epfl.ch

Declaration of Interests

The authors declare no competing interests.

Summary

Pancreatic Neuroendocrine Tumors (PanNETs) comprise two molecular subtypes, relatively benign islet tumors (IT) and invasive, metastasis-like primary (MLP) tumors. Hitherto, the origin of aggressive MLP tumors has been obscure. Herein, using multi-omics approaches, we revealed that MLP tumors arise from IT via dedifferentiation following a reverse trajectory along the developmental pathway of islet β-cells, which results in the acquisition of a progenitor-like molecular phenotype. Functionally, the microRNA-181cd cluster induces the IT-to-MLP transition by suppressing expression of the Meis2 transcription factor, leading to upregulation of a developmental transcription factor, Hmgb3. Notably, the IT-to-MLP transition constitutes a distinct step of tumorigenesis and is separable from the classical proliferation-associated hallmark, temporally preceding accelerated proliferation of cancer cells. Furthermore, PanNET patients with elevated HMGB3 expression and an MLP transcriptional signature are associated with higher-grade tumors and worse survival. Overall, our results unveil a new mechanism that modulates cancer cell plasticity to enable malignant progression.

Significance

Dedifferentiation has long been observed as a histopathological characteristic of many cancers, albeit inseparable from concurrent increases in cell proliferation. Herein we demonstrate that dedifferentiation is a mechanistically and temporally separable step in the multistage tumorigenesis of pancreatic islet cells, retracing the developmental lineage of islet beta cells.

Introduction

Pancreatic Neuroendocrine tumors (PanNETs) are rare human cancers that arise from the endocrine cells of the pancreas, the islets of Langerhans, and are broadly classified as 'functional' (secreting islet cell hormones, e.g., insulin) and 'non-functional' (NF-PanNETs) (1). According to the WHO, PanNETs are subdivided into three grades as G1, G2, and G3 based on the mitotic index and proliferation index (by *Ki-67*) (2,3). The majority of PanNETs are sporadic and typically exhibit alterations in the *MEN1* (~40%) and *DAXX/ATRX* (~35%) genes (4). Although novel therapies have improved the prognosis of low-grade PanNETs, high-grade tumors are invariably lethal (1), which motivates further efforts to better understand PanNET biology and the molecular programs that characterize high grade tumors.

Genetically engineered mouse models of cancer have been instrumental in understanding the underlying mechanisms of tumor progression. RIP1-Tag2 (RT2) is a prototypical mouse model of PanNET, in which the expression of SV40 T antigen in the insulin-producing pancreatic islet β-cells incapacitates p53 and Rb-family tumor suppressors, and leads to stepwise tumor development and progression (5). During tumorigenesis, a subset of hyperplastic islets, which appear between 4 to 6 weeks of age, undergo an angiogenic switch between 6 to 9 weeks, and a subset of these 'angiogenic islets' subsequently progress to form overt tumors. Histologically, the tumors are heterogeneous, representing either encapsulated solid tumors (adenomas) or invasive carcinomas, and a subset of cancer cells are capable of metastasizing to the lymph nodes and less frequently to the liver (5–7).

Using various transcriptomic data, we have previously reported three main molecular subtypes of human PanNETs, namely well-differentiated islet/insulinoma tumors (IT), 'intermediate' tumors, and poorly differentiated tumors associated with liver metastasis, called metastasis-like primary (MLP) (4,6,8). The IT subtype represents well-differentiated G1/2 PanNETs in humans, which are typically insulin secreting, non-invasive, and poorly metastatic. The human intermediate subtype also consists of well-differentiated tumors, both functional and non-functional, typically enriched for loss of the MEN1 tumor suppressor. The human MLP subtype is the most heterogeneous, and consists of non-functional and poorly-differentiated PanNET (grade G3), and around half have associated liver metastasis (8). Molecular subtyping analysis of the RT2 model revealed that a majority of tumors belong to the Insulinoma-like (IT) subtype, whereas a smaller subset presents as the more aggressive MLP subtype, which has the capability to metastasize to lymph nodes and liver (8,9). Despite lacking the mutational alterations that are present at varying frequencies in human PanNET (4), the IT and MLP tumors that arise in RT2 model have highly similar mRNA and miRNA transcriptome profiles to the human counterparts arguing that it is a valid model of human cancer (8). The human intermediate subtype is not phenocopied in the RT2 model, but rather in an engineered mouse model with β -cell specific inactivation of *Men1* tumor suppressor (10).

Previous studies have suggested two possible pathways for the development of the MLP subtype, based on descriptive analyses. The first proposed endocrine progenitors as the cell-of-origin for a separate tumorigenesis pathway leading to MLP tumors (6,8,11), whereas the second suggested

dedifferentiation to the MLP subtype from pre-existing cancer cells as the mechanism of malignant progression (7,12). In lieu of definitive functional studies, there has remained a lack of clarity about the molecular mechanism of malignant progression to G3/MLP tumors. The integration of high-throughput multi-omics data has proved to be a powerful resource for investigating molecular determinants of tumor development (13). In this study, we used multi-omics approaches to characterize the two main PanNET subtypes (i.e., insulinoma/IT and MLP), aiming to investigate the origin of the aggressive MLP subtype. To this end, we profiled primary and metastatic lesions of the RT2 mouse model of PanNET, integrating single-cell transcriptomics with bulk mRNA and miRNA sequencing and proteomic analysis, followed by functionally perturbing elements of a regulatory pathway implicated in specifying the development of the aggressive MLP subtype of PanNET.

Results

MLP PanNETs reactivate pancreatic β-cell progenitor signaling

To dissect the underlying genetic program of primary and metastatic PanNETs, we collected samples via laser-captured microdissection from primary tumors (31 samples) and liver metastases (6 samples) from the RIP1-Tag2 (RT2) genetically engineered mouse model in three different genetic backgrounds, as well as normal mouse pancreatic islets (4 samples), and normal mouse liver (3 samples) (Fig. 1A, Supplementary Fig. S1A to S1D, Supplementary Table 1). The collected samples – based on sufficient availability – were profiled for mRNA, miRNA, and proteomic analysis (Supplementary Fig. S1D). First, to assess the purity of the samples for cancer cells, we applied a cell-type deconvolution method – xCell (14) – to the samples that were subjected to RNA-sequencing analysis. This revealed a low level of immune- and stroma-scores, indicative of the high proportion of cancer cells in the bulk samples (Supplementary Fig. S1D). To evaluate the overall heterogeneity of the samples, we separately performed clustering analysis on all the samples from each platform, using the non-negative matrix factorization (NMF) method (15). Subsequently, a multi-omics clustering method – 'Similarity Network Fusion (SNF)' (16) – was applied to integrate information from the distinctive datasets – mRNA, miRNA, and protein. Since more samples were profiled for both mRNA and miRNA, in a separate analysis, we also applied SNF on the paired samples from these two datasets. The multi-omics clusters defined by SNF were highly concordant with the NMF clusters derived from a separate analysis of mRNA, miRNA, and proteomics profiles (Supplementary Fig. S1D).

In agreement with our previous reports (6,8), the tumors segregated into two broad subtypes with highly distinctive mRNA, miRNA, and proteomic profiles (Fig. 1A and Supplementary Fig. S1D). The first cluster, denoted as insulinoma/islet-tumors (IT), contained only primary tumors, which maintained high expression of well-defined markers of mature β-cells, including *Ins1/2*, *Insm1*, *Iapp*, *Nkx-6*, *Pax6*, *Pdx1*, and *Chga* (17,18), as detected in both transcriptomic (Supplementary Fig. S1E) and proteomic analyses (Fig. 1B). The second cluster, dubbed by Olson et al. (6) as 'metastasis-like primary' tumors (MLP), contained both primary and metastatic samples and were characterized by low expression of mature β-cell markers, along with an elevated expression of a number of endocrine progenitor markers (Fig. 1C and Supplementary Fig. S1F), including *Hmgb2/3*, *Fev*, and *Myc* (19). The Fisher exact test revealed no association between the IT and MLP phenotypes with the mouse strains from in which the tumors arose (Bl6 vs. AJ in all samples; p-value: 0.32, Bl6 vs. AJ in RNA-seq samples; p-value: 0.13).

To further characterize the MLP tumors, a miRNA signature and an mRNA signature for the MLP cluster were developed using differential expression analysis and NMF-selected features (see Methods). We identified a 28-member miRNA signature and a 203-member mRNA signature that each distinguished the IT and MLP subtype samples (Supplementary Table 1). Next, functional enrichment analyses (Gene Ontology terms, GO) for up- and downregulated genes in the MLP mRNA-signature were performed. Downregulated genes were enriched in GO-terms associated with

hormone secretion, pancreas development, cell-cell adhesion, and regulation of insulin secretion (Fig. 1D). The majority of the genes in these categories are involved in the homeostasis of mature β-cells, consistent with the observation that MLP tumors suppress mature β-cell markers.

Notably, repressors of cell differentiation and developmental processes were among the most significantly enriched GO-terms for upregulated genes in the MLP mRNA-signature (Fig. 1E). The MLP tumors had high expression of genes previously reported to be involved in maintaining stem-like features, playing essential roles in embryonic development and regeneration, and in the epithelial-to-mesenchymal transition, such as *Sox11* (20,21), *Sox6* (22), *Cited1* (23), *Id1* (24,25), and *Zfp536* (26) (Supplementary Table 1). These results are in agreement with our previous study by Sadanandam et al. (8), in which we observed higher expression of pancreatic progenitor-specific markers in MLP tumors (Fig. 1C, Supplementary Fig. S1F). Following up on this observation, we hypothesized that MLP tumors might have undergone dedifferentiation, thereby enabling the transition from IT to MLP subtype.

To begin assessing the dedifferentiation hypothesis, we leveraged pre-existing knowledge about islet β-cell differentiation from pancreatic progenitors to fully mature islet cells. Both human and mouse β-cells develop through three sequential phases of differentiation. Specifically, in mice, a primary transition takes place from E9.5 to E12.5, a secondary transition from E12.5 to birth, and finally, a postnatal maturation phase from birth to weaning (Fig. 1F, ref. (27–29)). Querying the presence of the MLP mRNA-signature in two separate datasets profiling the secondary transition (GSE8070) and the postnatal maturation of β-cells (19) revealed that the less differentiated pancreatic/β-cell samples had a higher MLP mRNA-signature score (Fig. 1G). These results indicated that the MLP transcriptome profile is active in normal β-cell progenitor cells. This observation was further substantiated by applying the MLP mRNA-signature onto a single cell profile of β-cell postnatal maturation (19), which showed a high correlation between the MLP gene-signature and less-differentiated states, independent of Mki67 proliferation marker (ANOVA p-value: 6.52e-23, Supplementary Fig. S1G to S1I). Furthermore, by applying the MLP microRNA-signature as a filter in an independent dataset profiling microRNA expression of pancreatic progenitor cells and mature β-cells (30), we again found enrichment of MLP microRNA expression in pancreatic progenitor cells (Fig. 1H).

Additionally, the enrichment analysis of upregulated genes revealed, among others, ‘neurogenesis/CNS development’ and ‘metabolic processes’ as highly enriched categories (Fig. 1E). Notably, these categories largely overlapped with the enrichment analysis of upregulated genes in embryonic E17.5 progenitors versus mature β-cells (Supplementary Fig. S1J). Concordantly, we have previously reported that PanNETs exploit neuronal synaptic signaling pathways to acquire invasive capabilities (31), and that altered cell metabolism is a feature of aggressive MLP tumors (8).

Next, we sought to evaluate the overall transcriptomic program of PanNETs further and assess the potential similarity between the two subtypes and the distinctive stages of β-cell differentiation. To

this end, the ComBat algorithm ("Combatting Batch Effects When Combining Batches of Gene Expression Microarray Data" (32)) was used to merge RNA-sequencing datasets describing the stages of mouse postnatal maturation (19) with those of tumor samples. Principal component analysis (PCA) on the merged dataset (Supplementary Fig. S1K) found PC2 as a highly correlated component with postnatal maturation time-points (ANOVA p-value: 0.00224, Fig. 1I); therefore, PC2 was considered as a proxy of the differentiation timeline trajectory. As expected, RNA samples from normal adult islets collected along with the PanNET tumors grouped closer to the dataset of mature (P60) β-cells. Notably, all samples from IT tumors grouped with intermediate-mature P9-P18 β-cells, and MLP samples clustered with P0-P3 immature β-cells, whereas (presumably more aggressive) metastatic samples clustered closer to the inception point of the β-cell differentiation trajectory (Fig. 1I).

Collectively, these results demonstrate that MLP tumors share characteristics with pancreatic progenitor cells and pose the intriguing hypothesis that MLP tumors emerge from the progression of IT cells via dedifferentiation and reactivation of progenitor-like signaling pathways.

MicroRNA-181cd induces the activation of the progenitor-like program in IT-like cell lines

To evaluate the hypothesis that dedifferentiation is a discrete step in tumorigenesis that gives rise to MLP tumors, we sought to identify signaling pathways that induce the MLP phenotype in IT-like cancer cells. MicroRNAs have been shown to regulate diverse signaling pathways and biological processes, including cellular reprogramming (33,34), and we have previously shown that a set of miRNAs is differentially expressed in MLP tumors compared to IT tumors (6,8). To identify candidate miRNAs with the potential to activate the MLP program in IT-like cell lines, the most highly upregulated MLP-associated miRNAs were sorted according to their correlation with the MLP-mRNA signature score in the RT2 tumor samples dataset (Supplementary Fig. S2A). Additionally, we segregated miRNAs that were differentially expressed between pancreatic progenitor cells and mature β-cells (Fig. 2A). This analysis led us to focus on two members of the miR-181 family, namely miR-181c and miR-181d, which compose the miR-181cd cluster (Fig. 2B).

To assess a possible functional role, the miR-181cd cluster was conditionally overexpressed in the βTC3 cell line, which showed IT-like phenotype (Supplementary Fig. S2B). To this end, we used a *piggy*Bac transposon system enabling doxycycline (DOX)-inducible miRNA expression (35). RNA-seq analysis was performed for collected samples at 24 hours and seven days after miR-181cd overexpression (Supplementary Fig. S2C and S2D), and activation of the progenitor-like program was evaluated by applying the MLP mRNA-signature onto the transcriptome profiles of the samples. Intriguingly, seven days of miR-181cd expression in the βTC3 IT-like cancer cells resulted in the transition of these cells toward the MLP subtype (Fig. 2C).

Congruently, IT marker genes, such as *Ins1*, *Ins2*, and *Iapp*, were downregulated upon miR-181cd expression, whereas various markers of MLP, including *Peg10*, members of ID family of transcriptional regulators, and the *Miat* long non-coding RNA, were amongst the upregulated genes

(Fig. 2D). Moreover, functional enrichment analysis of significantly upregulated genes after seven days of miR-181cd expression (Supplementary Table 2) revealed multiple GO-terms associated with neurogenesis and cell differentiation regulation as the most enriched categories (Fig. 2E).

In addition to a significant shift in the transcriptomic program and upregulation of genes involved in dedifferentiation, βTC3 cells underwent a morphological change upon induction of miR-181cd expression, characterized by the development of neuronal-like structures, similar to the morphology that is exhibited by the MLP-like cell line, AJ-5257-1 (Fig. 2F). These morphological changes were concordant with the enrichment of neurogenesis GO-term categories for upregulated genes both in the MLP subtype (Fig. 1E) and in β-cell progenitors (Supplementary Fig. S1G), as well as upregulated genes after seven days of miR-181cd expression (Fig. 2E). Additionally, we also evaluated the effect of miR-181cd expression in the 99-3o IT-like cell line (Supplementary Fig. S2B). Similar to the βTC3 cells, upon expression of miR-181cd in the 99-3o cells (Supplementary Fig. S2C and S2D), we observed downregulation of *Ins2*, an IT marker (Supplementary Fig. S2E), as well as morphological changes, which were accompanied by the appearance of neuronal-like structures (Supplementary Fig. S2F).

Although the βTC3 parental cells expressed higher endogenous levels of miR-181cd compared to the 99-3o cells (Supplementary Fig. S2C and S2D), overexpression of the miR-181cd transgene in both IT-like cell lines was necessary to induce gene expression and morphology changes that resemble the MLP subtype. We suspect that the comparatively higher levels of endogenous miR-181cd in the βTC3 vs. 99-30 cells might be due to sequestration by competitive endogenous RNAs in βTC3, much as has been reported for long-non coding RNAs (36,37). Irrespective, the results indicate that upregulated levels of miR-181cd are capable of instructing dedifferentiation from the IT to the MLP subtype.

Identification of transcription factors regulating the dedifferentiation from IT to MLP subtype

Next, we sought to explore the gene network underlying the IT-to-MLP transition and identify transcription factors (TFs) regulating the dedifferentiation process. To this end, an algorithm for the accurate reconstruction of cellular networks (ARACNe (38,39)) was employed to construct a transcriptional interaction map of RT2 PanNET tumors, and subsequently, a regulon analysis algorithm ('infer protein activity from single gene expression profiles,' VIPER (40)) was applied to identify candidate TFs controlling the IT-to-MLP transition (see Methods). VIPER implicated 66 and 72 TFs as potential positive or negative regulators of the MLP program, respectively (Supplementary Table 2).

First, we explored whether any of the TFs identified as prospective negative regulators might be potential targets of the miR-181cd cluster. To this end, a recently developed algorithm that enables the identification and ranking of biologically relevant miRNA targets (Bio-miRTa (35)) was used to query two datasets: (a) downregulated genes in the MLP signature and (b) downregulated genes in the miR-181cd overexpression experiment (Supplementary Table 2). *Meis2*, which encodes for a

homeobox protein that belongs to the three amino acid loop extension (TALE) family of homeodomain-containing proteins, ranked as the top miR-181cd gene target (Supplementary Fig. S3A). *Meis2* has been implicated in prostate cancer and neuroblastoma (41,42), and VIPER analysis revealed that the genes downstream of *Meis2* are also altered significantly between IT and MLP samples (Fig. 3A). Congruently, *Meis2* was downregulated upon forced miR-181cd expression in both βTC3 and 99-3o IT-like cell lines (Fig. 3B, and Supplementary Fig. S3B), as well as in MLP compared to IT tumors (Supplementary Fig. S3C). Using reporter assays, we verified the ability of miR-181cd to bind to the miRNA response element (MRE) in the 3'UTR of *Meis2* and trigger miRNA-mediated mRNA degradation (Fig. 3C and Supplementary Fig. S3D).

Then to identify and prioritize potential inducers of the IT-to-MLP dedifferentiation, we queried candidate TFs from the VIPER analysis in four mRNA datasets: (a) the secondary-transition phase of pancreatic development, (b) the β-cell postnatal maturation phase, (c) the dedifferentiation trajectory of primary cancer cells (PC2 in Fig. 1I), and (d) one resultant to miR-181cd overexpression in the β-TC3 IT-like cells (Supplementary Table 2). *Hmgb3*, an X-linked member of the high-mobility group box (HMGB) family, was the only gene that scored significantly high in all four datasets (Fig. 3D, Supplementary Fig. S3E-G), and the VIPER-inferred downstream genes of *Hmgb3* were also significantly altered comparing MLP to IT samples (Fig. 3A). Hmgb3 has been shown to modulate transcription, replication, recombination, DNA repair, and genomic stability (43), and its expression is associated with invasion, metastasis, and poor prognosis of a number of human cancers (44). Concordantly with these implications, *Hmgb3* was highly expressed in MLP samples at the mRNA and protein level (Supplementary Fig. S3H and S3I), and it was upregulated upon forced miR-181cd expression in the βTC3 and 99-3o IT-like cell lines (Fig. 3D and 3E, and Supplementary Fig. S3J and 3K).

Meis2 and Hmgb3 transcription factors regulate dedifferentiation to the MLP subtype

In order to assess the suspected regulatory pathway involving miR-181cd, *Meis2*, and *Hmgb3* in the transition from the IT to the MLP phenotype, an inducible miR-E-based shRNA knockdown system (as we have described previously in (45)) was used to downregulate the miR-181cd target, *Meis2*, in the IT-like ßTC3 cell line (Supplementary Fig. S3L). *Meis2* downregulation led to the upregulation of *Hmgb3* at the mRNA and protein level (Supplementary Fig. S3M and S3N), concomitant with downregulation of the IT marker *Ins2* (Supplementary Fig. S3O).

Next, to ascertain the role of *Hmgb3*, we used the *piggy*Bac (DOX)-inducible system to overexpress *Hmgb3* in the βTC3 cell line (Fig. 3F and Supplementary S3P). To characterize the effect of *Hmgb3* at the transcriptomic level in this IT-like cell line, RNA-seq analysis was performed for samples collected seven days after *Hmgb3* overexpression, as well as for control cells. Subsequently, by applying the MLP mRNA-signature to the transcriptome profiles, we observed that the βTC3 cell line transitioned toward the MLP subtype upon seven days of forced Hmgb3 expression (Fig. 3G). To assess the similarity in MLP gene network activation between the

overexpression of miR-181cd and *Hmgb3*, we merged the two datasets (see Methods) and ran hierarchical clustering on the merged MLP-mRNA gene expression matrix. Intriguingly, the result showed two main clusters, with the *Hmgb3* overexpression dataset clustering closest to the transcriptome profile of miR-181cd overexpression in βTC3 cell line (Fig. 3H).

Similar to miR-181cd, seven days of *Hmgb3* overexpression caused downregulation of IT markers such as *Ins2*, and *Nkx6-1* (Fig. 3I). Differential expression analysis of *Hmgb3*-overexpressing and control cells revealed increased expression of multiple genes involved in regulating neuronal programs, pluripotency, and cellular morphogenesis and migration (Supplementary Table 2 and Fig. 3I). Consistently, the majority of these genes are similarly upregulated by miR-181cd overexpression (Supplementary Fig. S3Q-U). Overall, these results establish *Hmgb3* as a key downstream effector of the miR-181cd-induced transition from IT cells to the dedifferentiated MLP subtype.

Hmgb3 is a marker of dedifferentiation and metastasis-like cells

Seeking to substantiate the evidence for dedifferentiation as a discrete regulatory event, we assessed the proposed miR-181cd/*Meis2*/*Hmgb3* axis *in vivo*. First, we immuno-stained tumor lesions for *Insulin* and *Hmgb3*, as well as for the oncoprotein T-antigen (to identify cancer cells) from two RT2 strains, i.e., AB/6J-F1 and C57Bl/6N, at early (7-9 weeks), middle (10-11 weeks), and advanced (14-16 weeks) stages of tumorigenesis. As expected, cancer cells (T-antigen^{+} cells) with *Ins*^{high}/*Hmgb3*$^{neg.}$ expression marked the IT tumors (Fig. 4A and Supplementary Fig. S4A). Notably, the initial downregulation of Insulin was coincident with *Hmgb3* upregulation, as indicated by the presence of *Ins*^{low}/*Hmgb3*^{high} cancer cells (Fig. 4A), which marked the transition from IT to MLP subtype emerging at the early stages of tumorigenesis. The IT-to-MLP transition was followed by complete loss of Insulin and high expression of *Hmgb3* in MLP lesions, indicated by *Ins*$^{neg.}$/*Hmgb3*^{high} cancer cells, both in early and late-stage primary tumors (Fig. 4A and Supplementary Fig. S4B). These results indicate that the induction of Hmgb3 is an early event in the dedifferentiation process of IT cancer cells into MLP subtype.

Examining the tumor sections from three different temporal stages of the disease showed an increase in the incidence of the IT-to-MLP and MLP lesions for both models during tumor progression (Supplementary Fig. S4C and S4D). Furthermore, when lymph node and liver metastases in the highly metastatic RT2;AB/6J-F1 model were examined, all lesions proved to be negative for the IT marker Insulin, and uniformly positive for Hmgb3, providing further evidence that Hmgb3 marks the aggressive and metastatic cancer cells of the MLP subtype, which consistently express this MLP marker, even after metastasizing and colonizing secondary parenchyma (Fig. 4B, Supplementary Fig. S4B and S4E).

Next, we sought to investigate the intra-tumoral heterogeneity at the single-cell level for IT and MLP subtypes in advanced lesions from the prototypical RT2;C57Bl6/N mouse model. Accordingly, two individual tumors were collected from two 14-week-old RT2 mice. The samples were processed

separately, and single-cell RNA sequencing (scRNA-seq) was performed for 2,375 individual cells in total. The clustering analysis was performed to identify and visualize the cells with similar expression patterns (see Methods and Supplementary Fig. S5A and S5B). Using known gene-markers (Supplementary Fig. S5C), we annotated different cell populations of the tumor microenvironment in primary PanNETs (Supplementary Fig. S5D), which revealed a similar ratio of various immune (infiltrating B- and T leukocytes, macrophages, and neutrophils) and stromal cell types (endothelial cells, pericytes, and cancer-associated fibroblast (CAFs)) in both primary tumor samples (Supplementary Fig. S5E).

Cancer cells were identified by expression of the SV40 large T-antigen oncogene and by a PanNET mRNA signature score comprising a 62-gene set diagnostic for transformed islet β-cells that was developed from the bulk RNA-seq data (Supplementary Fig. S5F and S5G, Supplementary Table 1). Clusters with average signature score above -0.4 were selected as cancer cells. Cluster 2 was excluded from the follow-up analysis due to low RNA-seq reads, and cluster 13 was excluded due to the low number of SV40 expressing cells. Although cluster 6 also scored highly for the PanNET signature, this cluster is comprised of macrophages (*Csf1r* positive cells; T-antigen negative, Supplementary Fig. S5H); and we envisage that phagocytosis incorporated the so-called "passenger" transcripts originating from engulfed apoptotic cancer cells (46). Accordingly, the cells within clusters 0, 1, 3, 4, and 5 were classified as cancer cells.

Next, clustering analysis was performed specifically for the selected cancer cells, which revealed seven distinct populations of cancer cells (cancer sub-clusters *i* to *vii*) with different transcriptome profiles (Fig. 4C and Supplementary Fig. S5I); both of the analyzed tumors showed a similar distribution in these sub-clusters (Supplementary Fig. S5J). Although cancer cells had variable level of SV40 expression, all sub-clusters demonstrated a similar level of the PanNET signature score (Supplementary Fig. S5K). Seeking to delineate cancer cells into IT vs. MLP subtypes, the MLP mRNA-signature was overlaid onto the single-cell transcriptome data. Sub-cluster *i* demonstrated the lowest MLP score, with high expression of mature β-cell markers such as *Ins2* (Fig. 4D, 4E, and Supplementary Fig. S5L). Relative to sub-cluster *i*, the rest of the six sub-clusters in the primary tumor demonstrated high activity of MLP transcriptomic program (Fig. 4D). Therefore, we concluded that sub-cluster *i* represents the IT cancer cells, and sub-clusters *ii* to *vii* are MLP cancer cells within primary tumors. Notably, we observed an inverse correlation of the *Meis2* and *Hmgb3* expression in the IT (sub-cluster *i*) and MLP cells (sub-clusters *ii* - *vii*) (Fig. 4E and Supplementary Fig. S5L), supporting our previous data implicating the Meis2/Hmgb3 axis in the IT-to-MLP transition.

Collectively, these results establish a miRNA/TF regulatory pathway, wherein miR-181cd induces downregulation of the *Meis2*, which leads to upregulation of *Hmgb3* expression. This pathway evidently plays an important role in the induction of the dedifferentiation process and the consequent transition of IT into MLP cancer cells, contributing thereby to the acquisition of invasive and metastatic capabilities (Fig. 4F).

Single-cell RNA-sequencing reveals a high proliferation rate in late-stage MLP tumors

Next, we used the PCA analysis on the transcriptomic data from the scRNA-seq to investigate the gene regulatory pathways contributing to the heterogeneity of the late-stage tumors. Considering the first two components of PCA (Fig. 5A and Supplementary Fig. S6A), PC-1 clearly showed a high correlation with the MLP mRNA-signature score, separating IT from MLP cancer cells (Fig. 5B and Supplementary Fig. S6B). Congruently, functional enrichment analysis on differentially expressed genes showed that the categories associated with the regulation of hormone and insulin secretion in normal β-cells were enriched in IT cancer cells (sub-cluster *i*, Fig. 5C, Supplementary Table 3). Conversely, categories related to cellular homeostasis, regulation of cell differentiation and CNS development were associated with MLP cancer cells (sub-clusters *ii* - *vii*, Fig. 5D, Supplementary Table 3).

Intriguingly, in addition to GO-terms representing MLP phenotype, the upregulated genes in MLP clusters exhibited high enrichment of functional categories associated with regulation of cell division and cell cycle (Fig. 5D, Supplementary Table 3). Therefore, we hypothesized that proliferation might be another major pathway contributing to the phenotypic state of cancer cells in the primary tumor. Accordingly, the second most variable component in the PCA analysis (PC-2) revealed a high correlation with cellular proliferation rate (Fig. 5E), with the highest significance for MLP cancer cells (sub-clusters *ii* - *vii*, cor.: 0.96, p-value < 2.2 e-16). Concordantly, the MLP clusters within the primary tumors exhibited different levels of proliferation capability (Fig. 5F) and *Mki67* expression (Supplementary Fig. S6C) showing the significant contribution of proliferation regulatory network in cellular heterogeneity of late-stage MLP cancer cells. Thus, the initial MLP sub-clusters *ii* and *iii* had a low proliferation score, whereas the progressive MLP sub-clusters *v*, *vi*, *vii* had a high score, with the intermediate sub-cluster *iv* highly variable, suggestive of a transition phase. Notably, the proliferation status of the cancer cells in these 7 sub-clusters was independent of the variable expression of the driving SV40 large T-antigen oncogene (Supplementary Fig. S6D and S6E).

In order to further investigate the sub-populations of MLP cancer cells, differential expression analysis was performed on each sub-cluster, followed by GO-term enrichment analysis (Supplementary Table 3). As expected, sub-cluster *i* showed a high expression of β-cell markers, including *Ins1/2*, *Nkx-6-1*, *Iapp*, and *Mafa* (Fig. 5G). On the other hand, sub-cluster *ii*, the first cluster with high expression of MLP signature genes (Supplementary Fig. S6B), was enriched in GO-terms representing negative regulation of differentiation (Supplementary Table 3). Interestingly, we observed upregulation of the islet α-cells gene markers *Gcg* (encoding for glucagon) and *Mafb* in sub-cluster *ii*. The switch from *Mafb* to *Mafa* expression is vital for islet β-cell maturation (28); hence, the transition from *Mafa* expression in sub-cluster *i* to *Mafb* expression in sub-cluster *ii* can be envisaged to signify the activation of dedifferentiation in cancer cells toward an endocrine progenitor-like state (Fig. 5G). Genes distinguishing sub-cluster *iii* proved to be involved in the G to S phase transition, as well as DNA repair and chromosomal stability, while sub-

cluster *iv* had the highest expression of genes associated with metabolism and hypoxia (Supplementary Table 3, Fig. 5G). This result suggests the presence of unfavorable conditions in the tumor microenvironment, such as hypoxia, experienced by a subset of MLP cancer cells. Finally, functional enrichment analysis for the differentially expressed genes in the last three sub-clusters (*v*, *vi*, *vii*) revealed cell division and cell cycle regulation as the most enriched categories (Fig. 5G, Supplementary Table 3). Most of the upregulated genes in these clusters were involved in the last phases of mitosis and G2 to M phase of the cell cycle, showing the hyperproliferative status of the cancer cells in these three sub-clusters (Fig. 5G).

These results collectively establish dedifferentiation and proliferation as the two qualitatively distinct cellular programs shaping the heterogeneity of late-stage primary tumors in the mouse model of PanNET.

Dedifferentiation precedes the activation of hyperproliferation during tumorigenesis

The hyperproliferative state of MLP cancer cells at advanced stages prompted us to investigate whether induction of dedifferentiation is temporally associated with substantive increases in the rate of cancer cell proliferation. Therefore, we examined the proliferation index of IT and MLP lesions in the early-stages of tumorigenesis by immunostaining the small, well-separated tumor lesions that are typical in young (8-10 week old) RT2;AB/6J-F1 mice. To this end, Insulin and Hmgb3 were used as biomarkers to distinguish IT and MLP subtypes, respectively, while EdU immunostaining marked proliferating cells. Notably, a similar number of proliferating cells was observed in both IT and MLP lesions in this early phase of tumor growth (Fig. 5H and 5I), indicating that dedifferentiation does not lead to an immediate increase in the proliferative capacity of cancer cells.

To further validate the immunostaining data, the effect of the miR-181cd expression on proliferation was examined by performing cell cycle analysis of βTC3 IT-like cancer cells seven days after miR-181cd overexpression. While overexpression of miR-181cd induced dedifferentiation in βTC3 cell line, we found no difference in proliferation status of the cells before and after miR-181cd induction (Fig. 5J and S5F). Concordantly, the GO-terms enrichment analysis of differentially expressed genes after seven days of miR-181cd expression did not show any categories associated with the cell cycle (see Fig. 3D). Overall, these results suggest that dedifferentiation is an early event in tumor progression, one that does not directly affect the proliferation capability of the cancer cells. This observation agrees with the previous data from the scRNA-seq analysis of islet β-cells during postnatal maturation that similarly revealed a dissociation between the β-cell differentiation program and proliferation (see Supplementary Fig. S1G to S1I).

Finally, we evaluated the proliferation rate in late-stage IT and MLP lesions from older (14–15-week-old) RT2 mice, again via immunostaining for Insulin, Hmgb3, and EdU. Consistent with the scRNA-seq data, late-stage MLP lesions showed a higher proliferation rate than late-stage IT lesions (Supplementary Fig. S6G-I). However, late-stage IT tumors exhibited a higher rate of proliferation compared to IT lesions in the early stage (Fig. 5I and Supplementary Fig. S6H). Collectively, these

data reveal that induction of the progenitor-like program is separable from and temporally precedes activation of the hyperproliferative signature in MLP cancer cells.

The MLP cluster in human PanNET is associated with higher grades, more frequent metastasis, and poor prognosis.

To investigate the possibility that the described dedifferentiation pathway and its regulators might be operative in human PanNET, we applied the MLP mRNA-signature onto a cohort of 110 human samples from both primary and metastatic tumors (47). Mirroring the approach used above to analyze mouse PanNET, RNA-sequencing datasets from mouse postnatal maturation (19), and human PanNETs (47) were merged. PCA analysis (Supplementary Fig. S7A) revealed that PC2 correlated with the postnatal maturation timeline trajectory of developing β-cells (Fig. 6A) (cor.: 0.53, p-value: 2.09e-09). Accordingly, human MLP tumors, identified by applying the mouse MLP mRNA-signature, were most similar to immature β-cells (Fig. 6A), suggesting that human cancer cells follow the same reverse developmental trajectory to acquire a progenitor-like phenotype that ostensibly contributes to increased malignancy.

Then we queried the MLP mRNA-signature in a cohort of 29 human tumor samples with available clinical follow-up data (4,48). The MLP signature had a significantly higher score in more aggressive human PanNETs, based on grade and T-stage (Fig. 6B and 6C). The MLP mRNA-signature was also assessed in a cohort of primary PanNETs and liver metastasis (47), which revealed a significantly higher signature score in metastatic samples (Supplementary Fig. S7B). Finally, the MLP mRNA-signature was associated with overall survival: patients with a high MLP score had poorer prognosis (Fig. 6D); in notable contrast, tumor grade and stage in the same cohort of patients did not have any predictive value (Supplementary Fig. S7C and S7D).

To assess the role of miR-181cd in tumor progression in the human disease, miRNA profiling of a cohort of human PanNETs (49) was used to examine the correlation of miR-181cd expression with clinicopathological features. Intriguingly, we found that high miR-181c and miR-181d expression was associated with more aggressive and non-functional PanNETs (Supplementary Fig. S7E-G).

Then, to explore the predicted anti-correlation of *MEIS2* and *HMGB3* in human PanNETs, their expression was assessed in the human PanNET datasets (4,47,48). Consistent with the data from the PanNET mouse model, we observed a significant negative correlation between the mRNA expression of these two transcription factors in human patients (Supplementary Fig. S7H). Interestingly, *MEIS2* and *HMGB3* expression exhibited negative and positive correlation with more aggressive tumors, respectively (Fig. 6E and 6F, Supplementary Fig. S7I and S7J). This result is in agreement with a previous report showing down-regulation of MEIS2 in metastatic pancreatic neuroendocrine neoplasm (50).

Furthermore, we used a cohort of archival human PanNETs tissue-microarrays (TMAs), which was immune-stained for HMGB3 protein. Congruently, HMGB3 positive sections were associated with

higher grade, T-stage and metastasis (Fig. 6G-I), suggesting that this transcription factor is also operative in specifying the human MLP PanNET subtype. Subsequently, we performed double immunostaining of the human PanNETs TMAs for the IT and MLP markers Insulin and HMGB3, respectively. The results revealed an anticorrelation for the two markers; high insulin-positive cells were HMGB3 negative, while insulin-negative cells were HMGB3 positive (Fig. 6J). Notably, similar to the mouse model, a small portion of cells had low expression of both markers, suggestive of an ongoing transition from IT to MLP phenotype (Fig. 6J; green arrows). Furthermore, we also observed interspersed IT (insulin-positive), and MLP (HMGB3-positive) cells in the same specimen, revealing intra-tumoral heterogeneity of human tumors with respect to IT and MLP subtypes (Supplementary Fig. S7K). Finally, the majority of liver metastases were negative for insulin while expressing high levels of Hmgb3 (Fig. 6K).

These results implicate miR-181/MEIS2/HMGB3-mediated dedifferentiation during malignant progression of human PanNETs to the more aggressive and metastatic MLP subtypes.

Discussion

Pancreatic Neuroendocrine Tumors (PanNETs) are histologically-diverse and oligo-mutated tumors lacking prevalent driving mutations in oncogenic signaling (1,4). Studies in mouse PanNET models have suggested two alternative tumorigenesis pathways leading to the predominant molecular and histopathologic subtypes, dubbed IT and MLP. One schematic envisioned parallel pathways, wherein β-cell progenitors were the cell-of-origin for the aggressive MLP subtype, and mature islet β-cell spawned benign insulinomas/islet tumors (IT) (6,8). The alternative scenario suggested dedifferentiation of relatively benign insulinomas/islet tumors (IT) into the invasive and metastatic MLP subtype (7). These alternative pathways were proposed based on comparative analyses of the molecular profiles of the IT and MLP tumors, but neither has been functionally validated so as to establish which mechanism is actually operative.

Although we cannot exclude the possibility that the aggressive MLP subtype can also arise directly from β-cell progenitor cells, herein we present compelling lines of evidence and functional validation that dedifferentiation and reactivation of a β-cell progenitor transcriptional program dictates the transition from the IT to the MLP subtype. First, our computational analysis of single-cell and bulk mRNA transcriptome profiling, and miRNA transcriptomic data, along with proteomic data, revealed a transition phase from IT to MLP tumors concordant with the activation of a β-cell progenitor-like program. Second, the miR-181cd cluster was identified as a regulatory factor that functionally contributes to the IT-to-MLP transition. Expression of the miR-181cd cluster was enriched both in normal pancreatic islet cell progenitors and in the MLP tumor subtype, and overexpression of miR-181cd in IT-like cancer cells activated a progenitor-like molecular phenotype and led to distinct morphological changes similar to the MLP subtype. Third, we uncovered elements of a regulatory circuit mediating dedifferentiation of PanNETs, in which the transcription factors *Meis2* and *Hmgb3* act as negative and positive regulators, respectively. Notably, *Meis2* is a direct target of miR-181cd, and its downregulation leads to the induction of *Hmgb3* expression. *Hmgb3* expression correlated both with β-cell progenitor stages and with the MLP signature, and its overexpression in an IT-like cell line similarly induced the IT-to-MLP transition. Concordantly, immunohistochemistry revealed a progressive increase in *Hmgb3* expression correlated with decreasing expression of the IT marker insulin, demonstrating a gradual phase transition from IT to MLP subtypes. Finally, LN and liver metastases were characterized by a complete loss of insulin expression and uniformly elevated expression of Hmgb3, consistent with the dependence of metastatic growth on the activation of this progenitor-like signaling pathway. The results establish the miR-181cd/*Meis2*/*Hmgb3*-axis as a key regulatory mechanism orchestrating the dedifferentiation program in PanNETs.

Furthermore, we validated our findings in different cohorts of human PanNETs, by demonstrating that the MLP signature, upregulation of miR-181cd and HMGB3, as well as downregulation of MEIS2, were all associated with aggressive tumors. Similar to the mouse PanNETs that develop *de novo* in RT2 mice, the MLP signature score in human PanNETs also correlated with pancreatic progenitors. Additionally, metastatic samples had higher expression of MLP-specific genes, and

patients bearing PanNET with high MLP-signature scores had worse prognosis. Notably, we also observed an anticorrelation of MEIS2 and HMGB3 expression, further substantiating the role of miR-181cd/MEIS2/HMGB3-axis in the dedifferentiation of human PanNETs.

Cellular plasticity enables cancer cells to evolve and activate ectopic programs in order to facilitate malignant progression (51). Dedifferentiation has been implicated but not functionally established as a discrete step in the progression of various cancers, such as melanoma (52), non-small cell lung (53,54), colorectal (55,56), breast (57,58), and pancreatic ductal adenocarcinoma (59,60). Herein we have revealed dedifferentiation to a progenitor-like state is a separable step in multistage tumorigenesis, wherein activation of the dedifferentiation transition to the MLP subtype does not directly alter cancer cell proliferation, which establishes dedifferentiation as an independent hallmark of aggressive tumors, one that is mechanistically separate from proliferation.

The human PanNET grading system currently used in the clinic is based on the proliferation index, characterized by the Ki67 histological marker, where poorly differentiated MLP-like neuroendocrine tumors show the highest $Ki67^{+}$ labeling index (>20% (61)). Our data reveal that initial dedifferentiation from IT-like cancer cells produces progenitor-like cells that are unaltered in their low proliferation index. Subsequently, the dedifferentiated cancer cells undergo dynamic evolution to a highly proliferative state that becomes predominant in MLP tumors. As such, some *bona fide* MLP lesions in human PanNET may not show a high proliferative index, despite the likely possibility of progressing in the future to the well-described highly-proliferative PanNET-G3 stage, indicating therefore that proliferation index may not be a fully informative marker of tumor grade. As such, incorporation of biomarkers of dedifferentiation, in particular Hmgb3, might offer added-value to the stratification of patients and better prediction of clinical outcomes.

Cancer cell progression coevolves with the tumor microenvironment (TME). This includes microvascular density (MVD), immune infiltration, and cancer-associated fibroblasts. In our previous study, we reported that the IT and MLP tumors have distinct MVD (8), while a recent study has shown that at least a subset of MLP in human PanNET patients exhibits high immune infiltration (62). The distinctive molecular profile of IT and MLP tumors warrants future studies to investigate reciprocal interaction between cancer cells and different cells within the TME and the roles that they play in the process of dedifferentiation and development of the MLP subtype.

Characterization of the miRNA transcriptome during multistep tumorigenesis of PanNET has previously revealed signature sets of differentially expressed miRNAs in the distinctive stages of PanNET tumorigenesis (6). We have recently shown two members of the MLP signature set, i.e. miR-137 and the miR-23b cluster, contribute to the invasive and metastatic capabilities of PanNETs (35). Specifically, the miR-23b cluster modulates the expression of ALK7, a receptor of the TGF-β superfamily, and a metastasis suppressor in PanNETs (45). Notably, ALK7 is one of the downregulated genes in MLP samples, which substantiates the link between the MLP phenotype and the evasion of homeostatic tissue barriers to tumor metastasis. In the present study, we have demonstrated that another member of the MLP signature set, the miR-181cd cluster, regulates a

distinctive parameter of the invasive and metastatic phenotype, namely dedifferentiation. The transcription factor *Hmgb3* was identified as an indirect downstream effector, demonstrably involved in the transition from IT to MLP subtype. *Hmgb3* has been previously implicated in maintaining the proper balance between hematopoietic stem cell (HSC) self-renewal and differentiation, wherein its expression inhibits the terminal differentiation of hematopoietic progenitor cells (63). These results motivate future investigations aimed to further chart the regulatory pathway, to identify upstream inducers of miR-181cd expression as well as downstream effectors of the miR-181cd/*Hmgb3*-mediated progenitor state operative in invasive and metastatic neuroendocrine pancreatic tumors.

The dedifferentiation process and activation of progenitor-like molecular phenotype in the MLP PanNETs were accompanied by the enrichment of neuronal gene sets that are also elevated in β-cell progenitors. Congruently, expression of miR-181cd in an IT-like cancer cell line led to morphological changes in the form of neuronal-like structures and activation of genes involved in neurogenesis. Interestingly, neurite outgrowth has been previously implicated in PanNET progression (64), and we have shown that PanNETs activate neuronal NMDAR signaling to acquire invasive capabilities (31,65), and that basal breast cancers activate the same pathway during brain metastasis (66). Neuronal pathways have also been implicated in neuroendocrine trans-differentiation in resistant tumors across different cancer types (67), and neuronal-like morphology such as axon-like protrusions linked to the malignant phenotype of small cell lung cancer (SCLC) (68). Thus, ectopic activation of neuronal signaling pathways may prove to be a broader mechanism involved in acquiring invasive and metastatic capabilities.

In summary, this work has established dedifferentiation as a discrete stepwise transition via which neuroendocrine cancer cells acquire progenitor-like features, contributing to malignant progression. The dedifferentiation pathway is demonstrably orchestrated by the upregulation of the miR-181cd cluster, which inhibits *Meis2* expression, leading in turn to the expression of *Hmgb3*. Identifying this network of progenitor-associated genes fills a conceptual gap in our understanding of the factors contributing to the specification of invasive and metastatic neuroendocrine pancreatic tumors, knowledge that could lay a foundation for therapeutic strategies aimed to hinder tumor progression and metastasis.

Author Contributions

S.S., I.P.M. and D.H. conceptualized and designed the study, and wrote the manuscript. S.S. and I.P.M. designed and performed experiments, and analyzed the results. S.S. designed and performed bioinformatic analyses. K.H. performed the single cell RNA-seq analysis. S.W. performed the proteomic sample collection and analysis. A.D.D. performed and analyzed NanoString data and scored the immunostaining on human PanNET TMAs. A.P. and I.M. provided the human PanNET TMAs and miRNA NanoString data and scored the immunohistochemistry. G.C. supervised the bioinformatic analysis. I.P.M. and D.H supervised the project. D.H. administered the project. All authors read and provided feedback on the manuscript.

Acknowledgment

We thank: G. Christofori (University of Basel), and E.F. Wagner and M. Farlik-Födinger (Medical University of Vienna) for insightful feedback and comments on the manuscript; S. Lamy, A. Etienne, M. Gaveta, L. Drori for technical support; M. Tichet for FACS analysis; J. Sordet-Dessimoz (Histology Core Facility–EPFL) for performing IHC; N. Zangger (Swiss Institute of Bioinformatics), S. Calderon (LGTF-UNIL), S. Pradervand (LGTF-UNIL) and B. Mangeat (Gene Expression Core Facility–EPFL) for assistance with RNA-seq analysis; and the EPFL School of Life Sciences BIOP, FCCF and HCF cores and animal care facility; and members of the Hanahan laboratory. This research was principally supported by a grant from the Swiss National Science Foundation (SNSF) to D.H. I.P.M. was supported in part by a Human Frontier Science Program Organization (HFSPO) fellowship.

Methods

Animal studies

All animals used in this study were maintained as a colony in a pathogen-free animal facility and all animal studies were approved by the Veterinary Authorities of the Canton Vaud according to Swiss Law. The following four RIP1-Tag2 (RT2) strains were used RT2;C57Bl6/N (RRID:IMSR_NCIMR:01XD5), RT2;C57Bl6/J (obtained by G. Christofori, University of Basel), RT2;A/J (RT2;C57Bl6/N were backcrossed to A/J mice for 10 generations), and the RT2;AB6F1 (F1 generation of A/J female mice crossed with male RT2;C57Bl6/J) (45).

Laser Capture Microdissection (LCM) sample collection

Tumor frozen sections were mounted onto PET-membrane slides (MMI). Sections were incubated with 70% ethanol and stained with cresyl violet. Each sample was microdissected using a PALM laser dissecting microscope (Zeiss). Serial sections from each lesion were used for the RNA or protein isolation:

- Total RNA was isolated using the QIAzol Lysis Reagent according to the instructions (QIAGEN, Cat. No. 217084).
- Total protein was extracted in 0.1% RapiGest SF Surfactant (Waters). Protein extracts were In-Solution digested as previously described (69). The reaction was stopped, and RapiGest cleaved by the addition of pure trifluoroacetic acid (TFA) during a final one-hour incubation at 37°C.

EdU cell proliferation assays

Mice were injected intraperitoneally with 100 µg of EdU in PBS. One hour post-injection, the mice were anesthetized using pentobarbital sodium and followed with transcardial perfusion with 20 ml of PBS, and then with 20 ml of 1% PFA.

Cell culture

All cell lines used in this study were maintained in a 5% CO_2 incubator at 37°C. The βTC3 cell line (RRID:CVCL_0172) was cultured in DMEM media containing 10% (v/v) Fetal Bovine Serum, and the AJ-5257-1 (ref: (45)) in DMEM-F12 media containing 10% (v/v) Fetal Bovine Serum, 1% (v/v) Insulin/transferrin/ Selenium, 4 mg/ml hydrocortisone and 5 mg/ml mouse EGF. Two mg/ml of doxycycline (DOX) was added to the media for the inducible miRNA/gene expression and knock-down experiments. The cell lines were tested to exclude Mycoplasma contamination via PCR by GATC Biotech every 12 months, and for all the experiments the cells were used within 5 passages after thawing.

Knockdown experiments

For the DOX-inducible gene knockdown experiments we used previously described PB-31 *piggy*Bac transposon vector (45), which allows for the expression of three tandem miR-E based shRNAs. The oligos for miR-E based shRNA are listed below:

- Meis2-shRNA-1:
    1. Meis2_17536_313_t:
    tcgagaaggtatatTGCTGTTGACAGTGAGCGCCACACGCAAAAACTATTTTAATA
    GTGAAGCCACAGATGTATTAAAATAGTTTTTGCGTGTGTTGCCTACTGCCTC
    GGActtcaaggggctag
    2. Meis2_17536_313_b:
    aattctagccccttgaagTCCGAGGCAGTAGGCAACACACGCAAAAACTATTTTAATA
    CATCTGTGGCTTCACTATTAAAATAGTTTTTGCGTGTGGCGCTCACTGTCAA
    CAGCAatataccttc
- Meis2-shRNA-2:
    1. Meis2_17536_353_t:
    tcgagaaggtatatTGCTGTTGACAGTGAGCGAAGATGTGACACTTAATATGAATA
    GTGAAGCCACAGATGTATTCATATTAAGTGTCACATCTGTGCCTACTGCCTC
    GGActtcaaggggctag
    2. Meis2_17536_353_b:
    aattctagccccttgaagTCCGAGGCAGTAGGCACAGATGTGACACTTAATATGAATA
    CATCTGTGGCTTCACTATTCATATTAAGTGTCACATCTTCGCTCACTGTCAA
    CAGCAatataccttc
- Meis2-shRNA-3:
    1. Meis2_17536_352_t:
    tcgagaaggtatatTGCTGTTGACAGTGAGCGACAGATGTGACACTTAATATGA
    TAGTGAAGCCACAGATGTATCATATTAAGTGTCACATCTGGTGCCTACT
    GCCTCGGActtcaaggggctag
    2. Meis2_17536_352_b:
    aattctagcccttgaagTCCGAGGCAGTAGGCACCAGATGTGACACTTAATATGA
    TACATCTGTGGCTTCACTATCATATTAAGTGTCACATCTGTCGCTCACTG
    TCAACAGCAatataccttc

MicroRNA cloning

The genomic area encompassing the miR-181c and miR-181d cluster (GRCm38/mm10 chr8:84,179,184-84,178,505) was PCR amplified from genomic DNA isolated from C57Bl6/N wild type mice. The Forward and Reverse primers (below) contained AttB1 and AttP1 sites to facilitate cloning in the pDNR221 vector, and subsequent subcloning to the PB-31 destination vector (45).

- Fwd-attB1-miR-181cd:
GGGGACAAGTTTGTACAAAAAAGCAGGCTCAGTTGTGAATGCATCCCTTG

- Rev-attB2-miR-181cd:
GGGGACCACTTTGTACAAGAAAGCTGGGTCATCTACCAGTTTGCCCACTG

Transfections

One million cells were plated in 6-well plates 24 hrs before transfection and the media was changed 2 hrs before transfections. For the transfection, the following liposomal complexes were set up:

- Single *piggy*Bac vector: 4.5 µg PB-1 + 1.5 µg PBase; 12 µl of Lipofectamine 2000
- Two *piggy*Bac vectors: 2.25 µg PB-1 + 2.25 µg PB-2 + 1.5 µg PBase; 12 µl of Lipofectamine 2000

The complexes were incubated for 20 min at room temperature and subsequently applied dropwise to the cells. The media was changed the next day, and stable cell lines were selected for resistance to Geneticin (G418; 1mg/ml) and/or Puromycin (2 µg/ml).

DNA synthesis

The coding area of mouse Hmgb3 transcript variant 2 (Gene Accession NM_008253) was purchased from OriGene (Hmgb3 Mouse Tagged ORF Clone, Cat#: MR202042). The Hmgb3 open-reading frame (ORF) was amplified using the primers shown below. The Kozak sequence GCCACCATG was included before the start codon in the Forward primer. AttB1 and AttP1 sites were also included to facilitate cloning in the pDNR221 vector, and subsequent subcloning to the PB-33 destination vector (45).

- Forward primer:
GGGGACAAGTTTGTACAAAAAAGCAGGCTGCCACCCGCGATCGCCATGGCTAAAG
G
- Reverse primer:
GGGGACCACTTTGTACAAGAAAGCTGGGTTCATTCATCTTCCTCCTCTTCCTCCTCC

Reporter assay

The Meis2 3'UTR (GRCm39/mm39 chr12:115,693,545-115,694,018) containing either the wild type or mutated miR-181 MRE were synthesized and subsequently cloned in the destination vector pcDHA-effLuc-RfA. The HEK293T cells (RRID:CVCL_0063) were stably transfected with the vector PB-13/PB-RB, allowing constitutive expression of the miR-181cd cluster. The reporter assays were performed as previously described in (35).

Cell cycle analysis

For this assay, the cells in suspension, as well as adherent cells were collected. The total number of $0.2*10^6$ cells were centrifuged and resuspended in 500 µl of 70% EtOH and incubated for 30 min in -20°C. Then the cells were centrifuged and washed with FACS buffer (PBS 2% FBS). Subsequently,

the cells were centrifuged again and then incubated staining buffer (FACS buffer, 20 µg/mL RNAse A (Invitrogen #12091-021), 40 µg/mL PI (Sigma #P4864-10ML)) for 15 min at room temperature.

mRNA extraction and cDNA synthesis

mRNA extractions from cultured cell lines were performed with the QIAGEN RNeasy kit (74106). Reverse transcription into cDNA was performed with PrimeScript RT Master Mix (Takara Bio Europe SAS) using five hundred nanograms of total RNA.

Real-time PCR for mRNA quantification

RT-PCR was carried out with primers designed according to the PrimerBank database (https://pga.mgh.harvard.edu/primerbank/index.html; RRID:SCR_006898) and synthesized by Microsynth AG, Balgach, Switzerland. All RT-PCR reactions were performed in triplicates using the 7900HT Fast RT-QPCT System (Applied BiosystemsTM).

- Ins2 forward primer: GCTTCTTCTACACACCCATGTC
- Ins2 reverse primer: AGCACTGATCTACAATGCCAC
- Meis2 forward primer: CAGGGTGGTCCAATGGGAATG
- Meis2 reverse primer: GGGGGTCCATGTCTTAACTGAG
- Rpl13 forward primer: AGCCGGAATGGCATGATACTG
- Rpl13 reverse primer: ATCTCACTGTAGGGCACCTCA

Real-time PCR for miRNA quantification

MystiCq® microRNA® SYBR® Green qPCR ReadyMix (cat. #: MIRRM02) was used to quantify miRNA expression levels in different cell lines. All the primers used for this analysis were ordered from MystiCq® microRNA qPCR kit as the following:

- miR-181c: mmu-miR-181c-3p (cat. #: MIRAP01276)
- miR-181d: has-miR-181d (cat. #: MIRAP00210)
- U6 (housekeeping miRNA): RNU6-1 (cat. #: MIRCP00001)

mRNA sequencing

RNA-seq libraries were prepared by first generating double-stranded cDNA from 10 ng total RNA with the NuGEN Ovation RNA-Seq System V2 (NuGEN Technologies, San Carlos, California, USA). 100 ng of the resulting double-stranded cDNA was fragmented to 350 bp using Covaris S2 (Covaris, Woburn, Massachusetts, USA). Sequencing libraries were prepared from the fragmented cDNA with the Illumina TruSeq Nano DNA Library Prep Kit (Illumina, San Diego, California, USA) according to the protocol supplied by the manufacturer. Cluster generation was performed with the libraries using the Illumina TruSeq SR Cluster Kit v4 reagents and sequenced on the Illumina HiSeq 2500 with TruSeq SBS Kit v4 reagents. Sequencing data were processed using the Illumina Pipeline Software version 1.82.

Purity-filtered reads were adapted and quality trimmed with Cutadapt (v. 1.2.1; RRID:SCR_011841). Reads matching to ribosomal RNA sequences were removed with fastq_screen (v. 0.11.1). The remaining reads were further filtered for low complexity with reaper (v. 15-065; RRID:SCR_009354). Reads were aligned against Mus musculus.GRCm38.86 genome using STAR (v. 2.5.3a; RRID:SCR_004463). The number of read counts per gene locus was summarized with htseq-count (v. 0.9.1; RRID:SCR_011867) using Mus musculus.GRCm38.86 gene annotation. The quality of the RNA-seq data alignment was assessed using RSeQC (v. 2.6.4; RRID:SCR_005275). Raw counts were further processed for normalization using DESeq2 pipeline (RRID:SCR_015687), where the data is normalized with the size factor to bring the count values to a common scale. This method is implemented in the R Bioconductor (RRID:SCR_006442) package DESeq2 (RRID:SCR_015687).

miRNA profile

The miRNA expression profiles were evaluated using the Agilent miRNA microarrays. Fluorescence was scanned with an Agilent G2566AA scanner and analyzed using the Feature Extraction 10.7.3.1 software. Normalization was performed on the Total Gene Signal from Agilent "GeneView" data files in R. Data were log2 transformed after adding a small constant (here: 4). Quantile normalization was performed using the "normalize.quantiles" function from R package "preprocessCore" from the Bioconductor project (ref. (70)).

Proteomics

Protein extracts from LCM samples were digested using the FASP procedure as previously described (ref. (71)). Peptides were desalted using StageTips (ref. (72)) and dried using a vacuum concentrator. For LC-MS/MS analysis, resuspended peptides were separated by reverse-phase chromatography on a Dionex Ultimate 3000 RSLC nano UPLC system connected in-line with an Orbitrap Fusion (Thermo Fisher Scientific, Waltham, USA). Raw data analysis was processed using MaxQuant 1.5.1.2 (RRID:SCR_014485), and database searches were performed against a human UniProt protein database.

The single-cell RNA sequencing

Single-cell tumor samples were freshly prepared. Tissues were cut with surgical scissors into 1 to 3 mm^3 cubes. The tissue was digested in a digestion mix with collagenase-I (25 mg) and collagenase-IV (25 mg) and DNAse-I (5 mg) in 10 ml HBSS. Tissue was digested for 30 to 40 min at 37°C in 5 ml digestion mix. After digestion, 35 ml of FACS buffer (2% BSA in 1x PBS) was added to the 5 ml digestion mix. This solution was passed through a 70 μM cell strainer and then centrifuged at 600 g for 5 min. The single-cell pellet was resuspended in 5 ml of 1x lysis buffer for 3 min. 35 ml of FACS buffer (2% BSA in 1x PBS) was added to the lysis buffer and centrifuged again at 600 g for 5 min. Cells were counted and diluted to 1 million cell/ml concentration. We used 10x Chromium standard 5' seq assay. We aimed at 3000 to 5000 cells final. The standard library preparation was done

following 10x Chromium protocol. Sequencing was done at a HiSeq4000 machine with the standard sequencing parameters (Read 1: 26 cycles, i7 index: 8 cycles, i5 index: 0 cycles, Read 2: 98 cycles).

Western blots

For western blotting, 10-20 µg of total protein extract were separated using sodium dodecyl sulfate-polyacrylamide gel electrophoresis and transferred onto PVDF blotting-membrane. Subsequently, the membranes were blocked with 5% Bovine Serum Albumin Fraction V (BSA) in TBS-T (pH 7.6; 0.5% Tween 20), and incubated with the primary and secondary antibodies diluted in 5% BSA in TBS-T. Finally, the membranes were visualized using ECL and imaged with Fusion FX7. The HMGB3 antibody (Abcam, ab75782; RRID:AB_1310317) and HSP90 antibody (Santa Cruz Biotechnology, SC-13119; RRID:AB_675659) were used in this study.

Immunostaining (mouse samples)

For immunostaining, the tissue sections were first dewaxed and rehydrated, and heat-induced epitope retrieval was done with 10 mM Sodium Citrate pH 6.0, followed by washing with PBS. The samples were incubated overnight at 4°C with antibodies diluted in 1% BSA. The next day, the samples were incubated for 40 min with the secondary Alexa Fluor antibodies (AlexaFluor488, AlexaFluor568, and AlexaFluor647; diluted according to the supplier's instruction). When needed, Tyramide Signal Amplification (TSA) revelation was done with AlexaFluor488. DAPI was used to stain the nuclei.

The immunofluorescence EdU was performed manually. After dewaxing and rehydration, sections were pretreated with heat in 10 mM Sodium citrate buffer pH 6 using the PT module (Thermo Fisher Scientific) for 20 min at 95°C. The primary antibodies were incubated overnight at 4°C under agitation. After three washes, the slides were incubated for 45 min with the secondary antibodies at RT. Tissue was treated with 0.5% Triton in PBS for 20 min at RT before incubation with the Azide reaction cocktail (0.1 M TBS pH7.4, 4 mM CuSo4, 100 mM Na-ascorbate, and 10 µM Azide Alexa594) to reveal the presence of EdU. The HMGB3 antibody (Abcam, ab75782; RRID:AB_1310317; dilution: 1:200), Insulin antibody (Dako A0564; dilution: 1:500) and SV40 T-antigen (in-house; dilution 1:1000) were used in this study.

Immunostaining (TMA cohort from human PanNETs)

Immunohistochemistry was performed on a TMA including 110 primary PanNETs and 62 metastases from patients who underwent surgery at the Inselspital Bern between 1990 and 2017. The study on this cohort was approved by the local ethics committees (KEK number 105/2015).

Sections of 2.5 µm were prepared from a TMA were used for staining with HMGB3 antibody (Abcam, ab75782; RRID:AB_1310317). Immunostaining was performed by automated staining using Bond RX (Leica Biosystems) immunostainer. All slides were dewaxed in Bond dewax solution (product code AR9222, Leica Biosystems) Heat-induced epitope retrieval at pH 9 in Tris buffer based (code AR9640, Leica Biosystems) for 30 min at 95°C. HMGB3 was diluted 1:200 and

incubated for 30 min. Samples were then incubated HRP (Horseradish Peroxidase)-polymer for 15 min and subsequently visualized using 3,3-Diaminobenzidine (DAB) as brown chromogen (Bond polymer refine detection, Leica Biosystems, Ref DS9800) for 10 min. HMGB3 was scored by a pathologist (A.P.) as negative, positive, and heterogeneous.

For the double HMGB3 and Insulin staining, the antibodies were incubated sequentially. Following on HMGB3 staining as described above, mouse Insulin antibody (Sigma Aldrich, I2018) was diluted 1:12000, incubated for 15 min. Secondary antibody, AP (Alkaline phosphatase)-polymer for 8 min, and visualized using fast red as red chromogen (Red polymer refine Detection, Leica Biosystems, Ref DS9390). Finally, the samples were counterstained with Haematoxylin and mounted with Aquatex (Merck). Slides were scanned and photographed using Pannoramic 250 (3DHistech).

Total RNA extraction – including small miRNA – from formalin-fixed human PanNETs

Total RNA extraction, including miRNAs, has been performed using the RecoverAll™ Total Nucleic Acid Isolation Kit for FFPE (Ambion; AM1975) according to the provider's instructions. DNA digestion via DNase has been performed during RNA isolation according to the manufacturer's instructions.

miRNA expression profiling on human PanNETs

We have analyzed miRNA expression from 24 PanNETs using the NanoString nCounter Human v3 miRNA Panel (NanoString Technologies, Seattle, USA) according to the manufacturer's instructions, 150 ng of total RNA have been used for running the assay. Normalization has been performed using the quantile normalization method (70). All the analyses have been performed within the R environment.

Image data acquisition and analysis

The entire tissue area of all slides was scanned using an Olympus slide scanner at 20x magnification, and the images were analyzed using the open-source software QuPath (RRID:SCR_018257). For quantifying the cells stained positive for a marker, we selected sections from different regions used "CellIntensityClassifications" method, as described in ref. (73).

Clustering analysis

For subtype identification, we applied the NMF algorithm ("NMF" package in R, ref. (15)) on each profiling platform (i.e., mRNA, lncRNA, miRNA, and protein), separately. For clustering, we selected the top 25% most variable genes (features) from the normalized datasets. The Cophenetic coefficient was used to select the optimized number of clusters for each analysis. The features contributing the most to each cluster were also extracted using "extractFeatures" function in the R package.

SNF algorithm (ref. (16)) was applied for multi-omics clustering. The top 25% of the most variable features in mRNA, lncRNA, miRNA, and proteomics were used as an input for the algorithm. We used “SNFtool" package in R for running this analysis, and we applied the default setting in the package. Estimating the most optimal number of clusters was done using "estimateNumberOfClustersGivenGrap” function. For a better resolution on the final clustering, we excluded the normal pancreatic and liver samples from this analysis. The final clusters were manually curated and annotated, based on single platform NMF clustering in addition to SNF results.

Differential expression analysis

For mRNA differential expression analysis, we used DESeq pipeline (DESeq2 R package; RRID:SCR_015687), where the data is modeled with a negative binomial distribution to estimate the dispersion and fold changes. For extracting the differential expressed genes, we consider the samples’ mouse strain as covariates to remove its effect on the downstream analysis. The cutoffs for gene selection were adjusted p-value < 0.01 and Fold change > 1.5.

As for the differential miRNA expression was assessed using the limma package (RRID:SCR_010943), p-values were adjusted using the Benjamini–Hochberg method and significance cut-off set at 0.05. We selected miRNA with greater than 1.5 fold change.

Subtype signature development

The MLP mRNA-signature was generated based on the result of differential expression analysis of mRNA and lncRNA datasets (IT samples vs. MLP samples). We also included the genes that were identified as the contributing features for NMF clustering in both mRNA and lncRNA datasets. Furthermore, we also checked in the protein analysis to see which of the genes differentially expressed have a similar trend in the proteomics data and a control dataset.

Likewise, the miRNA signature was generated by the union of the differential expressed miRNA (IT vs. MLP samples), and features contributing to the NMF clustering in the miRNA dataset.

PanNET signature development

The 62-mRNA signature for transformed islet β-cells (PanNET signature) was generated from the bulk RNA-seq data following these criteria:

1. Differentially upregulated genes in IT and MLP tumors vs normal islet β-cells (fold change > 4; adjusted p-value < 0.01)
2. Excluding the genes that were also differentially expressed between IT and MLP tumor samples.
3. Excluding the genes that are involved in cell cycle regulation (genes in Cell-Cycle GO term)

Cross-species analysis

To merge different datasets and correct for the batch effects, we employed ComBat ("sva " package in R; RRID:SCR_010974). For merging human and mouse datasets, the HUGO gene nomenclature was used as the reference.

Single-cell RNA sequencing data analysis

We used the Cell Ranger pipeline (version 3.1; RRID:SCR_017344) for processing the raw data. The downstream analysis was performed using Seurat package in R (RRID:SCR_007322). Cells were filtered based on the number of features from 200 to 7500, percentage of mitochondrial genes <10%. We used all standard Seurat setting for normalization, PCA, tSNE analysis, and clustering.

Single-cell clusters' annotation

Gene expression levels of different markers used to identify the cell-type population in the tumor microenvironment: *SV-40*; cancer cells, *Ins2*; ß-cells and cancer cells, *Cd3e:* T-cell Leukocytes, *Cd19* & *Ms4a1*: B-cell Leukocytes, *Pecam1*: Endothelial cells, *Csf3r*: Neutrophils, *Csf1r*: Macrophages, *Mrc1*: M2 macrophages, *Mfap5*: CAFs, *Acta2*: Pericytes.

We also used the total number of features for the cells to filter out the cancer cells having a significantly lower number of detected features (<2500). This cluster was called "Tumor low-reads" and was excluded from the downstream analysis of cancer cells.

Differential expression analysis in scRNA-seq data

Differential expression analysis between clusters were performed using the Wilcoxon rank-sum test, using 0.05 as the cut-off for adjusted p-value, and 1.5 for the average fold change in expression level. Then the genes were sorted based on average fold-change and the top 20 were selected for clusters' marker genes. In the case of IT vs. MLP analysis, the top 100 genes were kept and reported.

Proliferation signature score for scRNA-seq data

To estimate the proliferation capability of the single cells, we used a signature of G2M marker genes provided by Seurat R package (V.3.2; RRID:SCR_007322).

PanNET regulator network

The regulatory network was constructed using the ARACNe package (RRID:SCR_002180) from 54 samples from RT2 mouse model. We ran ARACNe with 100 bootstrap iterations using all the genes in the dataset and the parameters were set to 0.15 DPI (Data Processing Inequality) tolerance and MI (Mutual Information) P value threshold of 10^{-7}.

Transcription factor regulators of IT to MLP transition

The candidate transcription factors regulating IT-to-MLP transition were inferred using VIPER analysis as described in (40). The differential expression analysis for all the genes in the datasets was

performed according to the package manual at Bioconductor, by comparing IT to MLP samples identified from the clustering analysis. For selecting the transcription factor from the list of VIPER-inferred regulators we used a list of 1636 Mus-musculus TF reported at (74).

Gene Ontology (GO) terms enrichment analysis

GO Terms enrichment analysis was performed using the online web service based on the Molecular Signatures Database (MSigDB; RRID:SCR_016863). Enriched GO terms were defined as GO biological process (BP) obtaining an FDR-adjusted P-value < 0.05, retrieving a maximum of 50 terms.

Gene signature enrichment analysis

Single sample Gene Set Enrichment Analysis (ssGSEA, ref. (75)), implemented in the R package GSVA, was used to calculate an expression score for each gene expression signature and each sample. The method that was used to estimate the gene-set enrichment scores were specified to "ssgsea" in GSVA package.

Correlation analysis

To evaluate the degree of correlation between two continuous variables, we employed "cor" function in R to retrieve the Pearson correlation coefficient. For the significance estimation of the extracted correlation, we used "lm" function in R for linear modeling the data and retrieved FDR-adjusted P values.

Survival analysis

Kaplan–Meier survival analysis was used to assess the relationship of the signature scores with overall survival. We applied the Large-sample Chi-square test (log-rank test) to determine the associations between predictor variables and to obtain adjusted hazard-ratios. These analyses were performed with the R package ''survival.''

Quantification and statistical analysis

All statistical analyses described above were performed with R.

Data availability

RNA sequencing data and regulon analysis presented in this study are deposited at ZENODO database (RRID:SCR_004129), and are accessible via https://doi.org/10.5281/zenodo.4160441

References

1. Zhou C, Zhang J, Zheng Y, Zhu Z. Pancreatic neuroendocrine tumors: A comprehensive review. Int. J. Cancer. 2012;131:1013–22.

2. Rindi G, Klimstra DS, Abedi-Ardekani B, Asa SL, Bosman FT, Brambilla E, et al. A common classification framework for neuroendocrine neoplasms: an International Agency for Research on Cancer (IARC) and World Health Organization (WHO) expert consensus proposal. Mod Pathol. 2018;31:1770–86.

3. Tang LH, Untch BR, Reidy DL, O'Reilly E, Dhall D, Jih L, et al. Well-differentiated neuroendocrine tumors with a morphologically apparent high-grade component: A pathway distinct from poorly differentiated neuroendocrine carcinomas. Clin Cancer Res. 2016;22:1011–7.

4. Scarpa A, Chang DK, Nones K, Corbo V, Patch AM, Bailey P, et al. Whole-genome landscape of pancreatic neuroendocrine tumours. Nature. 2017;543:65–71.

5. Hanahan D. Heritable formation of pancreatic β-cell tumours in transgenic mice expressing recombinant insulin/simian virus 40 oncogenes. Nature. 1985;315:115–22.

6. Olson P, Lu J, Zhang H, Shai A, Chun MG, Wang Y, et al. MicroRNA dynamics in the stages of tumorigenesis correlate with hallmark capabilities of cancer. Genes Dev. 2009;23:2152–65.

7. Perl AK, Wilgenbus P, Dahl U, Semb H, Christofori G. A causal role for E-cadherin in the transition from adenoma to carcinoma. Nature. 1998;392:190–3.

8. Sadanandam A, Wullschleger S, Lyssiotis CA, Grötzinger C, Barbi S, Bersani S, et al. A cross-species analysis in pancreatic neuroendocrine tumors reveals molecular subtypes with distinctive clinical, metastatic, developmental, and metabolic characteristics. Cancer Discov. 2015;5:1296–313.

9. Chun MGH, Mao JH, Chiu CW, Balmain A, Hanahan D. Polymorphic genetic control of tumor invasion in a mouse model of pancreatic neuroendocrine carcinogenesis. Proc Natl Acad Sci U S A. 2010;107:17268–73.

10. Bertolino P, Tong WM, Herrera PL, Casse H, Zhang CX, Wang ZQ. Pancreatic β-cell-specific ablation of the multiple endocrine neoplasia type 1 (MEN1) gene causes full penetrance of insulinoma development in mice. Cancer Res. 2003;63:4836–41.

11. Cejas P, Drier Y, Dreijerink KMA, Brosens LAA, Deshpande V, Epstein CB, et al. Enhancer signatures stratify and predict outcomes of non-functional pancreatic neuroendocrine tumors. Nat Med.; 2019;25:1264–9.

12. Title AC, Hong SJ, Pires ND, Hasenöhrl L, Godbersen S, Stokar-Regenscheit N, et al. Genetic dissection of the miR-200–Zeb1 axis reveals its importance in tumor differentiation and invasion. Nat Commun.; 2018;9:4671.

13. Frost HR, Amos CI. A multi-omics approach for identifying important pathways and genes in human cancer. BMC Bioinformatics. 2018;19:479.

14. Aran D, Hu Z, Butte AJ. xCell: Digitally portraying the tissue cellular heterogeneity landscape. Genome Biol. 2017;18:220.

15. Brunet JP, Tamayo P, Golub TR, Mesirov JP. Metagenes and molecular pattern discovery using matrix factorization. Proc Natl Acad Sci U S A. 2004;101:4164–9.

16. Wang B, Mezlini AM, Demir F, Fiume M, Tu Z, Brudno M, et al. Similarity network fusion for aggregating data types on a genomic scale. Nat Methods. 2014;11:333–7.

17. Baron M, Veres A, Wolock SL, Faust AL, Gaujoux R, Vetere A, et al. A Single-Cell Transcriptomic Map of the Human and Mouse Pancreas Reveals Inter- and Intra-cell Population Structure. Cell Syst. 2016;3:346-360.e4.

18. Teo AKK, Lim CS, Cheow LF, Kin T, Shapiro JA, Kang NY, et al. Single-cell analyses of human islet cells reveal de-differentiation signatures. Cell Death Discov. 2018;4:14.

19. Qiu WL, Zhang YW, Feng Y, Li LC, Yang L, Xu CR. Deciphering Pancreatic Islet β Cell and α Cell Maturation Pathways and Characteristic Features at the Single-Cell Level. Cell Metab. 2017;25:1194-1205.e4.

20. Miao Q, Hill MC, Chen F, Mo Q, Ku AT, Ramos C, et al. SOX11 and SOX4 drive the reactivation of an embryonic gene program during murine wound repair. Nat Commun. 2019;10:4042.

21. Sock E, Rettig SD, Enderich J, Bösl MR, Tamm ER, Wegner M. Gene Targeting Reveals a Widespread Role for the High-Mobility-Group Transcription Factor Sox11 in Tissue Remodeling. Mol Cell Biol. 2004;24:6635–44.

22. Jiang W, Yuan Q, Jiang Y, huang L, Chen C, Hu G, et al. Identification of Sox6 as a regulator of pancreatic cancer development. J Cell Mol Med. 2018;22:1864–72.

23. Murphy AJ, Pierce J, de Caestecker C, Ayers GD, Zhao A, Correa H, et al. CITED1 confers stemness to wilms tumor and enhances tumorigenic responses when enriched in the nucleus. Oncotarget. 2014;5:386–402.

24. Tamari K, Konno M, Asai A, Koseki J, Hayashi K, Kawamoto K, et al. Polyamine flux suppresses histone lysine demethylases and enhances ID1 expression in cancer stem cells. Cell Death Discov. 2018;4:104.

25. Sun Y, Lai X, Yu Y, Li J, Cao L, Lin W, et al. Inhibitor of DNA binding 1 (ID1) mediates stemness of colorectal cancer cells through the id1-c-Myc-PLAC8 axis via the wnt/β-catenin and shh signaling pathways. Cancer Manag Res. 2019;11:6855–69.

26. Qin Z, Ren F, Xu X, Ren Y, Li H, Wang Y, et al. ZNF536, a Novel Zinc Finger Protein

Specifically Expressed in the Brain, Negatively Regulates Neuron Differentiation by Repressing Retinoic Acid-Induced Gene Transcription. Mol Cell Biol. 2009;29:3633–43.

27. Benitez CM, Goodyer WR, Kim SK. Deconstructing pancreas developmental biology. Cold Spring Harb Perspect Biol. 2012;4:1–17.

28. Hang Y, Stein R. MafA and MafB activity in pancreatic β cells. Trends Endocrinol Metab. 2011;22:364–73.

29. Yu X, Qiu W, Yang L, Zhang Y, He M, Li L, et al. Defining multistep cell fate decision pathways during pancreatic development at single-cell resolution. EMBO J. 2019;38:e100164.

30. Jacovetti C, Matkovich SJ, Rodriguez-Trejo A, Guay C, Regazzi R. Postnatal β-cell maturation is associated with islet-specific microRNA changes induced by nutrient shifts at weaning. Nat Commun. 2015;6:8084.

31. Li L, Hanahan D. Hijacking the neuronal NMDAR signaling circuit to promote tumor growth and invasion. Cell. 2013;153:86–100.

32. Johnson WE, Li C, Rabinovic A. Adjusting batch effects in microarray expression data using empirical Bayes methods. Biostatistics. 2007;8:118–27.

33. Bartel DP. Metazoan MicroRNAs. Cell. 2018;173:20–51.

34. Vidigal JA, Ventura A. The biological functions of miRNAs: Lessons from in vivo studies. Trends Cell Biol. 2015;25:137–47.

35. Michael IP, Saghafinia S, Hanahan D. A set of microRNAs coordinately controls tumorigenesis, invasion, and metastasis. Proc Natl Acad Sci. 2019;116:201913307.

36. Yu H, Dong L, Wang H, Zhang Y, Wang Z, Wang C, et al. Linc00504 promotes the malignant biological behavior of breast cancer cells by upregulating hmgb3 via decoying microrna-876-3p. Cancer Manag Res. 2021;13:1803–15.

37. Peng W, Si S, Zhang Q, Li C, Zhao F, Wang F, et al. Long non-coding RNA MEG3 functions as a competing endogenous RNA to regulate gastric cancer progression. J Exp Clin Cancer Res. 2015;34:79.

38. Basso K, Margolin AA, Stolovitzky G, Klein U, Dalla-Favera R, Califano A. Reverse engineering of regulatory networks in human B cells. Nat Genet. 2005;37:382–90.

39. Margolin AA, Nemenman I, Basso K, Wiggins C, Stolovitzky G, Favera RD, et al. ARACNE: An algorithm for the reconstruction of gene regulatory networks in a mammalian cellular context. BMC Bioinformatics. 2006;7:S7.

40. Alvarez MJ, Shen Y, Giorgi FM, Lachmann A, Ding BB, Hilda Ye B, et al. Functional characterization of somatic mutations in cancer using network-based inference of protein activity.

Nat Genet. 2016;48:838–47.

41. Bhanvadia RR, Van Opstall C, Brechka H, Barashi NS, Gillard M, McAuley EM, et al. MEIS1 and MEIS2 expression and prostate cancer progression: A role for HOXB13 binding partners in metastatic disease. Clin Cancer Res. 2018;24:3668–80.

42. GroB A, Schulz C, Kolb J, Koster J, Wehner S, Czaplinski S, et al. Tumorigenic and antiproliferative properties of the TALE-transcription factors MEIS2D and MEIS2A in neuroblastoma. Cancer Res. 2018;78:1935–47.

43. Štros M. HMGB proteins: Interactions with DNA and chromatin. Biochim. Biophys. Acta. 2010;1799:101–13.

44. Song N, Liu B, Wu JL, Zhang RF, Duan L, He WS, et al. Prognostic value of HMGB3 expression in patients with non-small cell lung cancer. Tumor Biol. 2013;34:2599–603.

45. Michael IP, Saghafinia S, Tichet M, Zangger N, Marinoni I, Perren A, et al. ALK7 Signaling Manifests a Homeostatic Tissue Barrier That Is Abrogated during Tumorigenesis and Metastasis. Dev Cell. 2019;49:409-424.e6.

46. Lantz C, Radmanesh B, Liu E, Thorp EB, Lin J. Single-cell RNA sequencing uncovers heterogenous transcriptional signatures in macrophages during efferocytosis. Sci Rep. 2020;10:14333.

47. Alvarez MJ, Subramaniam PS, Tang LH, Grunn A, Aburi M, Rieckhof G, et al. A precision oncology approach to the pharmacological targeting of mechanistic dependencies in neuroendocrine tumors. Nat Genet. 2018;50:979–89.

48. Missiaglia E, Dalai I, Barbi S, Beghelli S, Falconi M, Della Peruta M, et al. Pancreatic endocrine tumors: Expression profiling evidences a role for AKT-mTOR pathway. J Clin Oncol. 2010;28:245–55.

49. Di Domenico A, Pipinikas CP, Maire RS, Bräutigam K, Simillion C, Dettmer MS, et al. Epigenetic landscape of pancreatic neuroendocrine tumours reveals distinct cells of origin and means of tumour progression. Commun Biol. 2020;3:1–11.

50. Hansel DE, Rahman A, House M, Ashfaq R, Berg K, Yeo CJ, et al. Met proto-oncogene and insulin-like growth factor binding protein 3 overexpression correlates with metastatic ability in well-differentiated pancreatic endocrine neoplasms. Clin Cancer Res. 2004;10:6152–8.

51. Yuan S, Norgard RJ, Stanger BZ. Cellular plasticity in cancer. Cancer Discov. 2019;9:837–51.

52. Köhler C, Nittner D, Rambow F, Radaelli E, Stanchi F, Vandamme N, et al. Mouse Cutaneous Melanoma Induced by Mutant BRaf Arises from Expansion and Dedifferentiation of Mature Pigmented Melanocytes. Cell Stem Cell. 2017;21:679-693.e6.

53. Lin SC, Chou YT, Jiang SS, Chang JL, Chung CH, Kao YR, et al. Epigenetic switch between

SOX2 and SOX9 regulates cancer cell plasticity. Cancer Res. 2016;76:7036–48.

54. Winslow MM, Dayton TL, Verhaak RGW, Kim-Kiselak C, Snyder EL, Feldser DM, et al. Suppression of lung adenocarcinoma progression by Nkx2-1. Nature. 2011;473:101–4.

55. Fumagalli A, Oost KC, Kester L, Morgner J, Bornes L, Bruens L, et al. Plasticity of Lgr5-Negative Cancer Cells Drives Metastasis in Colorectal Cancer. Cell Stem Cell. 2020;26:569-578.e7.

56. Ordóñez-Morán P, Dafflon C, Imajo M, Nishida E, Huelsken J. HOXA5 Counteracts Stem Cell Traits by Inhibiting Wnt Signaling in Colorectal Cancer. Cancer Cell. 2015;28:815–29.

57. Bach K, Pensa S, Grzelak M, Hadfield J, Adams DJ, Marioni JC, et al. Differentiation dynamics of mammary epithelial cells revealed by single-cell RNA sequencing. Nat Commun. 2017;8:2128.

58. Giraddi RR, Chung CY, Heinz RE, Balcioglu O, Novotny M, Trejo CL, et al. Single-Cell Transcriptomes Distinguish Stem Cell State Changes and Lineage Specification Programs in Early Mammary Gland Development. Cell Rep. 2018;24:1653-1666.e7.

59. Krah NM, De La O. JP, Swift GH, Hoang CQ, Willet SG, Pan FC, et al. The acinar differentiation determinant PTF1A inhibits initiation of pancreatic ductal adenocarcinoma. Elife. 2015;4:e07125.

60. Shi G, Direnzo D, Qu C, Barney D, Miley D, Konieczny SF. Maintenance of acinar cell organization is critical to preventing Kras-induced acinar-ductal metaplasia. Oncogene. 2013;32:1950–8.

61. Scarpa A, Mantovani W, Capelli P, Beghelli S, Boninsegna L, Bettini R, et al. Pancreatic endocrine tumors: Improved TNM staging and histopathological grading permit a clinically efficient prognostic stratification of patients. Mod Pathol. 2010;23:824–33.

62. Young K, Lawlor RT, Ragulan C, Patil Y, Mafficini A, Bersani S, et al. Immune landscape, evolution, hypoxia-mediated viral mimicry pathways and therapeutic potential in molecular subtypes of pancreatic neuroendocrine tumours. Gut. 2020;gutjnl-2020-321016.

63. Nemeth MJ, Kirby MR, Bodine DM. Hmgb3 regulates the balance between hematopoietic stem cell self-renewal and differentiation. Proc Natl Acad Sci U S A. 2006;103:13783–8.

64. Cavallaro U, Niedermeyer J, Fuxa M, Christofori G. N-CAM modulates tumour-cell adhesion to matrix by inducing FGF-receptor signalling. Nat Cell Biol. 2001;3:650–7.

65. Li L, Zeng Q, Bhutkar A, Galván JA, Karamitopoulou E, Noordermeer D, et al. GKAP Acts as a Genetic Modulator of NMDAR Signaling to Govern Invasive Tumor Growth. Cancer Cell. 2018;33:736-751.e5.

66. Zeng Q, Michael IP, Zhang P, Saghafinia S, Knott G, Jiao W, et al. Synaptic proximity enables

NMDAR signalling to promote brain metastasis. Nature. 2019;573:526–31.

67. Balanis NG, Sheu KM, Esedebe FN, Patel SJ, Smith BA, Park JW, et al. Pan-cancer Convergence to a Small-Cell Neuroendocrine Phenotype that Shares Susceptibilities with Hematological Malignancies. Cancer Cell. 2019;36:17-34.e7.

68. Yang D, Qu F, Cai H, Chuang CH, Lim JS, Jahchan N, et al. Axon-like protrusions promote small cell lung cancer migration and metastasis. Elife. 2019;8:e50616.

69. Chopra T, Hamelin R, Armand F, Chiappe D, Moniatte M, McKinney JD. Quantitative mass spectrometry reveals plasticity of metabolic networks in mycobacterium smegmatis. Mol Cell Proteomics. 2014;13:3014–28.

70. Bolstad BM, Irizarry RA, Åstrand M, Speed TP. A comparison of normalization methods for high density oligonucleotide array data based on variance and bias. Bioinformatics. 2003;19:185–93.

71. Wiśniewski JR, Zougman A, Nagaraj N, Mann M. Universal sample preparation method for proteome analysis. Nat Methods. 2009;6:359–62.

72. Rappsilber J, Mann M, Ishihama Y. Protocol for micro-purification, enrichment, pre-fractionation and storage of peptides for proteomics using StageTips. Nat Protoc. 2007;2:1896–906.

73. Bankhead P, Loughrey MB, Fernández JA, Dombrowski Y, McArt DG, Dunne PD, et al. QuPath: Open source software for digital pathology image analysis. Sci Rep. 2017;7:16878.

74. Hu H, Miao YR, Jia LH, Yu QY, Zhang Q, Guo AY. AnimalTFDB 3.0: A comprehensive resource for annotation and prediction of animal transcription factors. Nucleic Acids Res. 2019;47:D33–8.

75. Barbie DA, Tamayo P, Boehm JS, Kim SY, Moody SE, Dunn IF, et al. Systematic RNA interference reveals that oncogenic KRAS-driven cancers require TBK1. Nature. 2009;462:108–12.

Figure legends:

Figure 1: The aggressive MLP subtype of PanNET has a similar expression profile to islet β-cell progenitors

A. Multi-omics clustering of samples isolated via LCM from primary tumors and liver metastasis from the RT2 mice, as well as pancreatic islets and liver from wild type mice, in the C57Bl6/N, C57Bl6/J, and A/J genetic backgrounds. Samples of the IT and MLP subtype are colored as green and red, respectively.

B-C. Heatmaps of protein levels, detected by mass spectrometry from LCM samples, of mature β-cell markers (B) and endocrine progenitor markers (C) in IT and MLP PanNET tumor samples.

D-E. Gene Ontology (GO) categories significantly enriched (FDR q-value on the y-axis) for downregulated (D) and upregulated (E) genes in the MLP transcriptome signature.

F. Schematic representation of mouse endocrine pancreas development depicting the stages from early progenitors (E9.5) to fully mature β-cells (P60).

G. Score of the MLP mRNA signature in different embryonic stages during the secondary transition of mouse pancreatic development (left panel) and postnatal maturation (right panel). In both datasets there MLP score declines in the curse of differentiation.

H. The MLP miRNA signature scores are high in endocrine pancreatic progenitor cells (E10), but not in mature β-cells.

I. PCA analysis of samples from the temporal mouse pancreatic islet postnatal maturation phase compared to primary tumors and liver metastasis from the RT2 mouse model along with normal (non-transgenic) islets. The x-axis shows PC2, which represents a surrogate for dedifferentiation time-points. The samples from each cohort are separated in different rows (see also Supplementary Fig. S1K.)

Figure 2: MicroRNA-181cd induces dedifferentiation when upregulated in IT cancer cells

A. Heatmap of differentially expressed MLP-signature miRNAs comparing mature β-cells and pancreatic progenitor cells from wild-type mice.

B. Scatter plot showing the correlation between miR-181c (top) and miR-181d (bottom) expression (x-axis) and the MLP mRNA signature score (y-axis) in RT2 PanNET tumor samples.

C. MLP mRNA-signature scores in cell cultures collected 24 hours and 7 days following induction of miR-181cd expression in the βTC3 IT-like cancer cell line, which reveals a transcriptional shift toward MLP after 7 days.

D. Heatmap of MLP mRNA-signature genes in miR-181cd transfected βTC3 cells, which indicates that the majority of upregulated MLP genes (colored coded as red in the y-axis) were upregulated after 7 days of miR-181cd expression; conversely, the genes downregulated in the MLP signature (colored coded as green in the y-axis) were congruently downregulated after 7 days of miR-181cd expression. Selected IT and MLP gene markers are identified on the right side (see Supplementary Table 2 for the list of genes in order).

E. Gene Ontology (GO) categories that were significantly enriched (FDR q-value on the y-axis) for upregulated genes after 7 days of miR-181cd cluster overexpression in βTC3 cells.

F. Brightfield images of cancer cells: i. βTC3 IT-like cells; ii. βTC3 cells transfected with miR181cd cluster after 2 weeks of expression induced with DOX; iii. AJ-5257-1 MLP-like cells. Lower right panel: Magnified image illustrating miR-181cd-induced neuronal-like structures (in dashed lines) in ßTC3 cells.

Figure 3: The axis miR-181cd/Meis2/Hmgb3 regulates the IT to MLP transition

A. The Meis2 and Hmgb3 transcription factors (TFs) were identified as potential TF regulators using VIPER. Red and blue vertical lines indicate genes induced and repressed, respectively, by each TF.

B. mRNA expression levels of Meis2 upon DOX-induced overexpression of miR-181cd in ßTC3.

C. Luciferase reporter assay shows the direct targeting of Meis2 mRNA by miR-181cd.

D. Hmgb3 mRNA expression in ßTC3 cells upon DOX-induced overexpression of miR-181cd.

E. Protein expression level of Hmgb3 in the AJ-5257-1 cell line as well as in ßTC3 upon DOX-induced miR-181cd overexpression.

F. Hmgb3 protein expression levels in ßTC3cells upon DOX-induced Hmgb3 overexpression.

G. MLP mRNA-signature scores in βTC3 cancer cells collected 7 days after the induction of Hmgb3 expression, which shows a transcriptional shift toward the MLP phenotype.

H. Unsupervised hierarchical clustering of βTC3 cells before (control) and after miR-181cd or Hmgb3 induction for 7 days.

I. Heatmap of selected differentially expressed genes in βTC3 cell lines before (control) and after 7 days of Hmgb3 overexpression, reflecting pathways related to neuroendocrine phenotype, neuronal programming, pluripotency, and morphogenesis (see Supplementary Table 2 for the complete list of genes).

Figure 4: Hmgb3 upregulation is an early event in the dedifferentiation of IT into MLP

A, B. Representative images of Insulin and Hmgb3 immunostaining, alongside DAPI, of early pancreatic tumors (A) and liver metastasis (B) in the RT2;AB/6J F1 mouse model of PanNETs.

A. Representative images of early lesions showing: IT cells; identified as $Ins^{high}/Hmgb3^{neg.}$ (left panel), cells undergoing IT-to-MLP transition; identified as $Ins^{high}/Hmgb3^{low}$ and $Ins^{low}/Hmgb3^{high}$ (middle panels), and fully dedifferentiated MLP cells; identified as $Ins^{neg.}/Hmgb3^{high}$ (right panel) (see also Supplementary Fig. S4A-D).

B. Metastatic cancer cells exhibit $Ins^{neg.}/Hmgb3^{high}$ expression pattern (see also Supplementary Fig. S4E).

C. t-distributed Stochastic Neighbor Embedding (t-SNE) analysis for all cancer cells based on scRNA- sequencing analysis, color coded according the seven distinct sub-clusters.

D. Individual cancer cells (points) in two-dimensional t-SNE plots, color-coded according to the MLP signature score.

E. mRNA expression levels of Ins2 (left), Meis2 (middle), and Hmgb3 (right) in scRNA-sequencing data from primary tumor samples.

F. Schematic representation of dedifferentiation process during PanNETs tumor progression: The IT cancer cells ($Ins^{high}/Hmgb3^{neg.}$) go through dedifferentiation and transition to MLP subtype ($Ins^{neg.}/Hmgb3^{high}$), enabling them to disseminate to the liver. This transition is induced by upregulation of miR-181cd, which directly inhibits Meis2 expression, and indirectly effects the upregulation of Hmgb3 expression.

Figure 5: Dedifferentiation and proliferation are two separate molecular pathways contributing to the heterogeneity of primary tumors

A. Principal component analysis (PCA) of all cancer cells based on scRNA- sequencing analysis, color coded according to the cell sub-clusters.

B. Scatter-plot showing a high correlation of PC-1 from the PCA analysis and the MLP mRNA-signature score.

C-D. Gene Ontology (GO) categories that are significantly enriched (FDR q-value on the y-axis) for upregulated genes in sub-cluster *i* (C; IT cancer cells), and in sub-clusters *ii* to *vii* (D; MLP cancer cells).

E. Scatter-plot showing a high correlation of PC-2 from PCA analysis with the mRNA proliferation-signature score for both IT (sub-cluster *i*) and MLP clusters (sub-clusters *ii* - *vii*).

F. Violin plot showing the mRNA proliferation-signature score for each cancer cell sub-cluster.

G. Heatmap of top 20 differentially expressed genes for each cancer cell sub-cluster in the primary tumor.

H. Images of Insulin, Hmgb3, and EdU immunostaining, along with DAPI, for early lesions from 7-8 week old RT2;AB/6J-F1 mice, illustrating representative IT, MLP and transitional histological stages.

I. Quantification of EdU immunostaining to reveal proliferation of cancer cells in IT and MLP tumor lesions isolated from early, 7-8 week old, RT2;AB/6J-F1 mice.

J. Cell cycle analysis of ßTC3 cells before (control) and after 7 days of miR-181cd DOX-induced expression.

Figure 6: The MLP cluster in human PanNETs correlates with dedifferentiation, tumor grade, metastasis, and clinical outcome

A. PCA analysis of samples from mouse pancreatic postnatal maturation and human PanNET primary tumors and liver metastasis. The PC2 is shown in the x-axis as a surrogate for dedifferentiation time-points. The samples from each cohort are separated in different rows.

B, C. The MLP mRNA signature scores in low- and high-grade (B) and different stages (C) of human PanNETs.

D. Association of overall survival of PanNET patients with a high MLP signature score (score > median, red line) versus low score (score < median, green line).

E, F. MEIS2 (E) and HMGB3 (F) mRNA expression in different stages of human PanNETs.

G-I. Association of HMGB3 protein expression in human PanNET tissue-microarrays (TMA) with clinicopathological features.

J, K. Representative images of Insulin (identified by red cytoplasm) and HMGB3 (marked by brown nucleus) immunostaining of primary human PanNETs (J) and liver metastases (K).

J. In the middle panels, red arrowheads denote the IT subtype; $INS^{high}/HMGB3^{neg.}$ cells; green arrows the IT-to-MLP transition; $INS^{low}/HMGB3^{low}$ cells, and black arrows the MLP subtype; $INS^{neg.}/HMGB3^{high}$ cells.

Figure 1

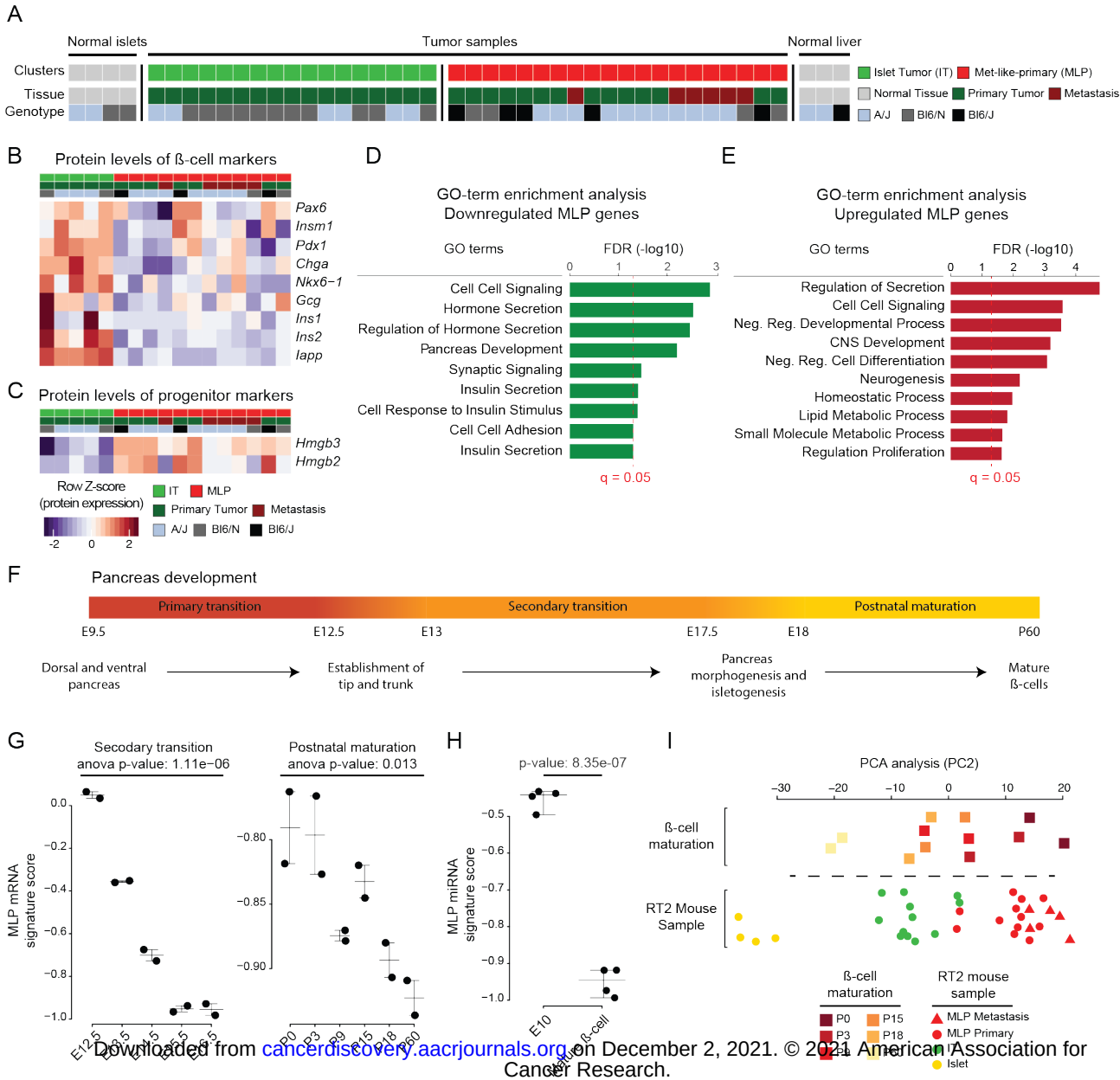

Figure 2

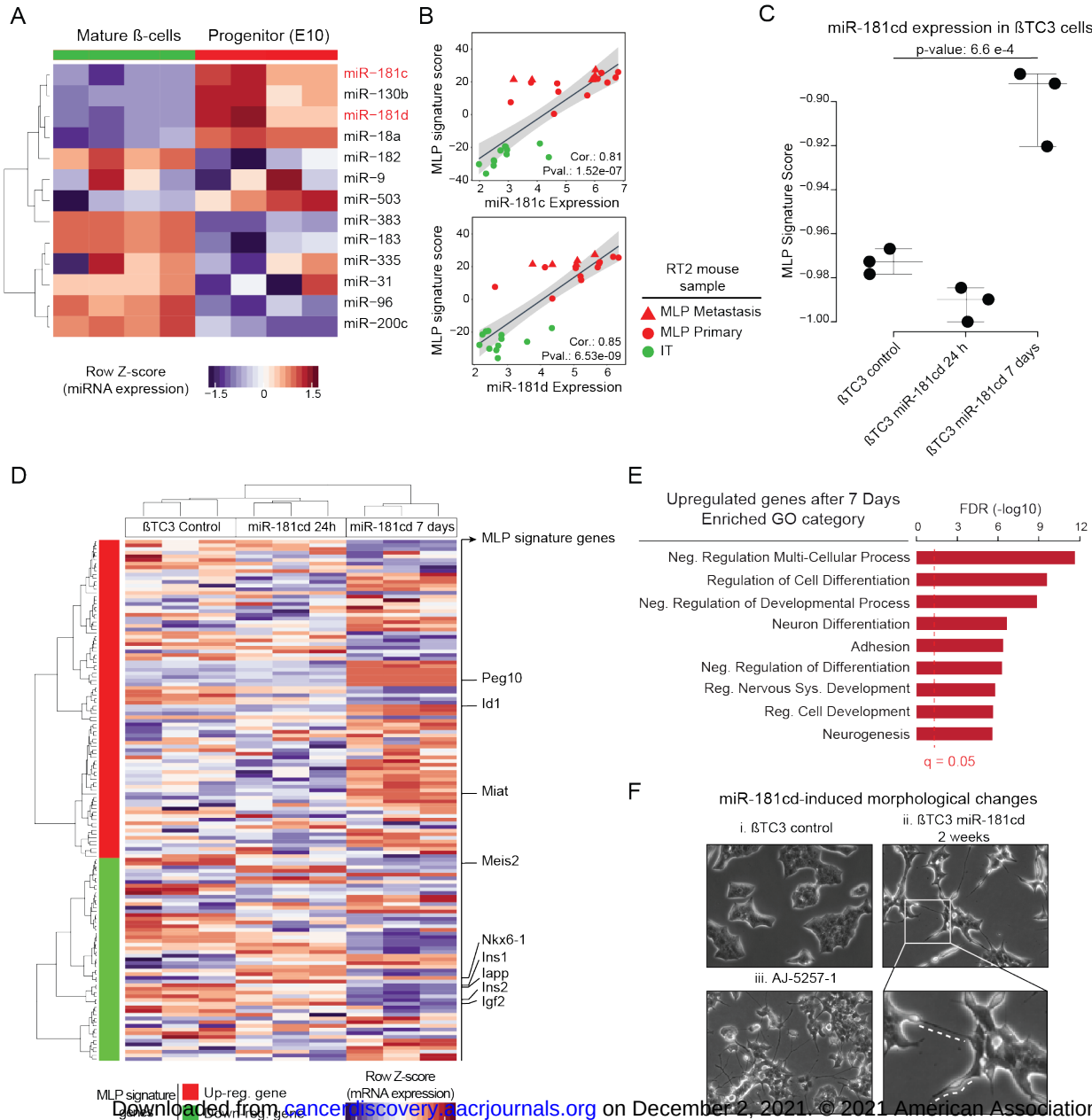

Figure 3

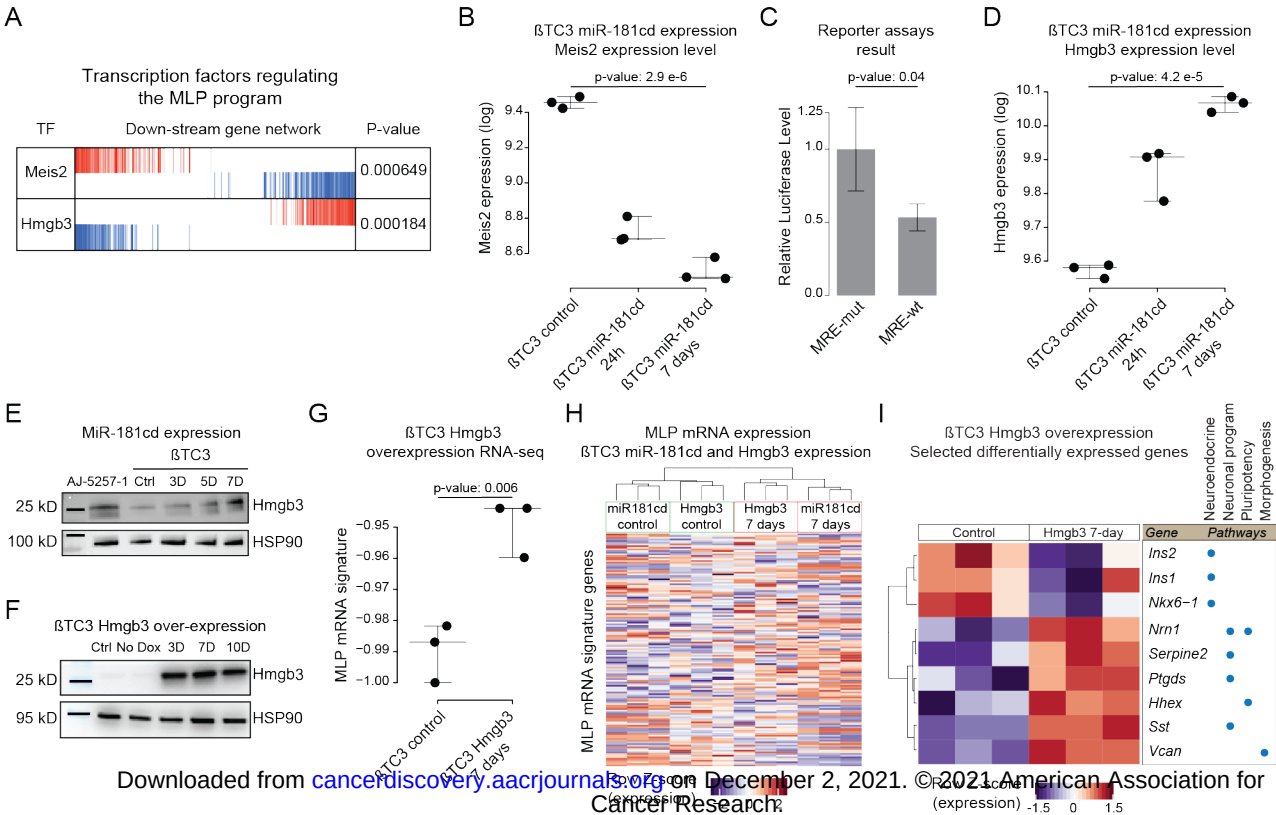

Figure 4

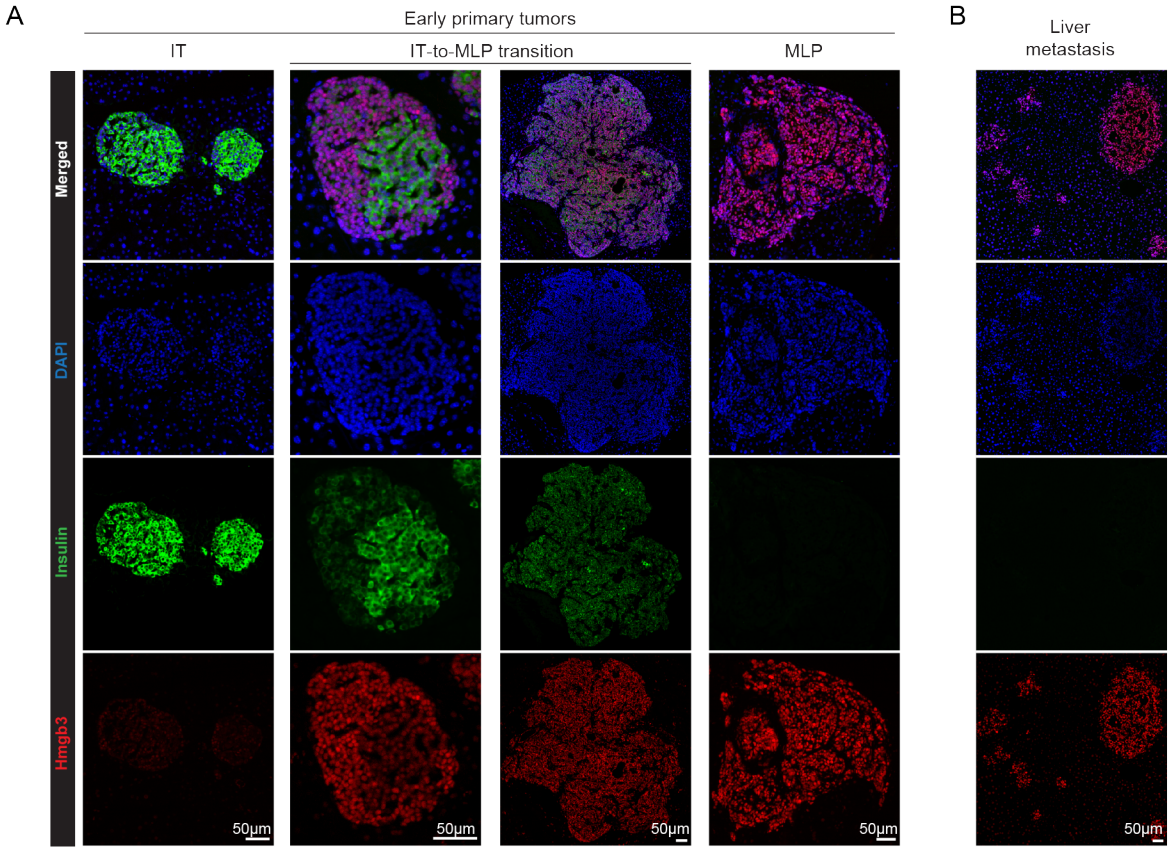

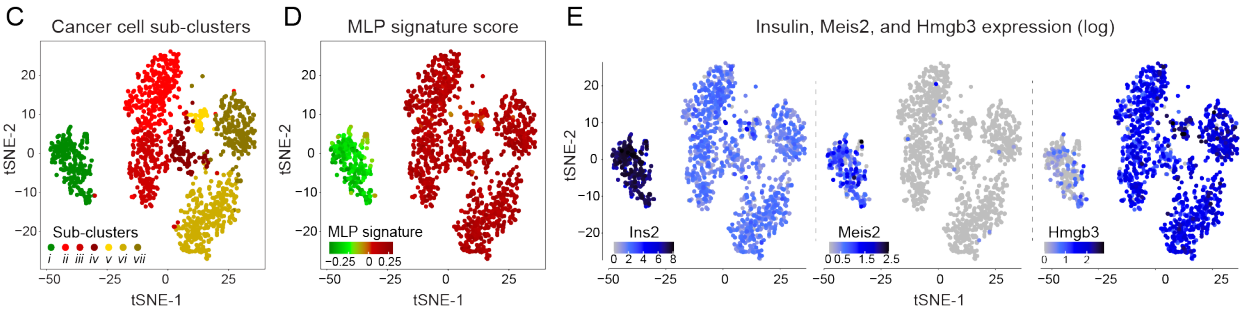

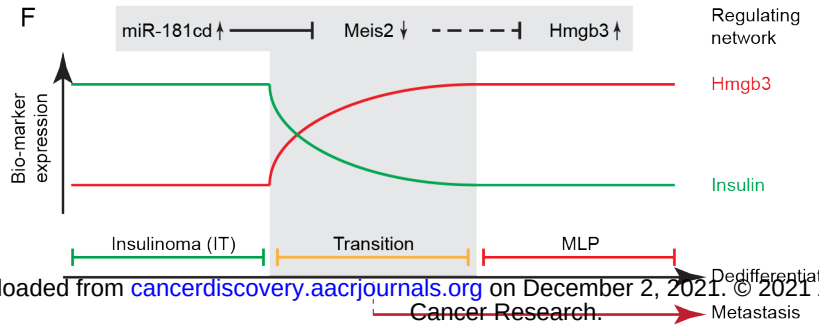

Figure 5

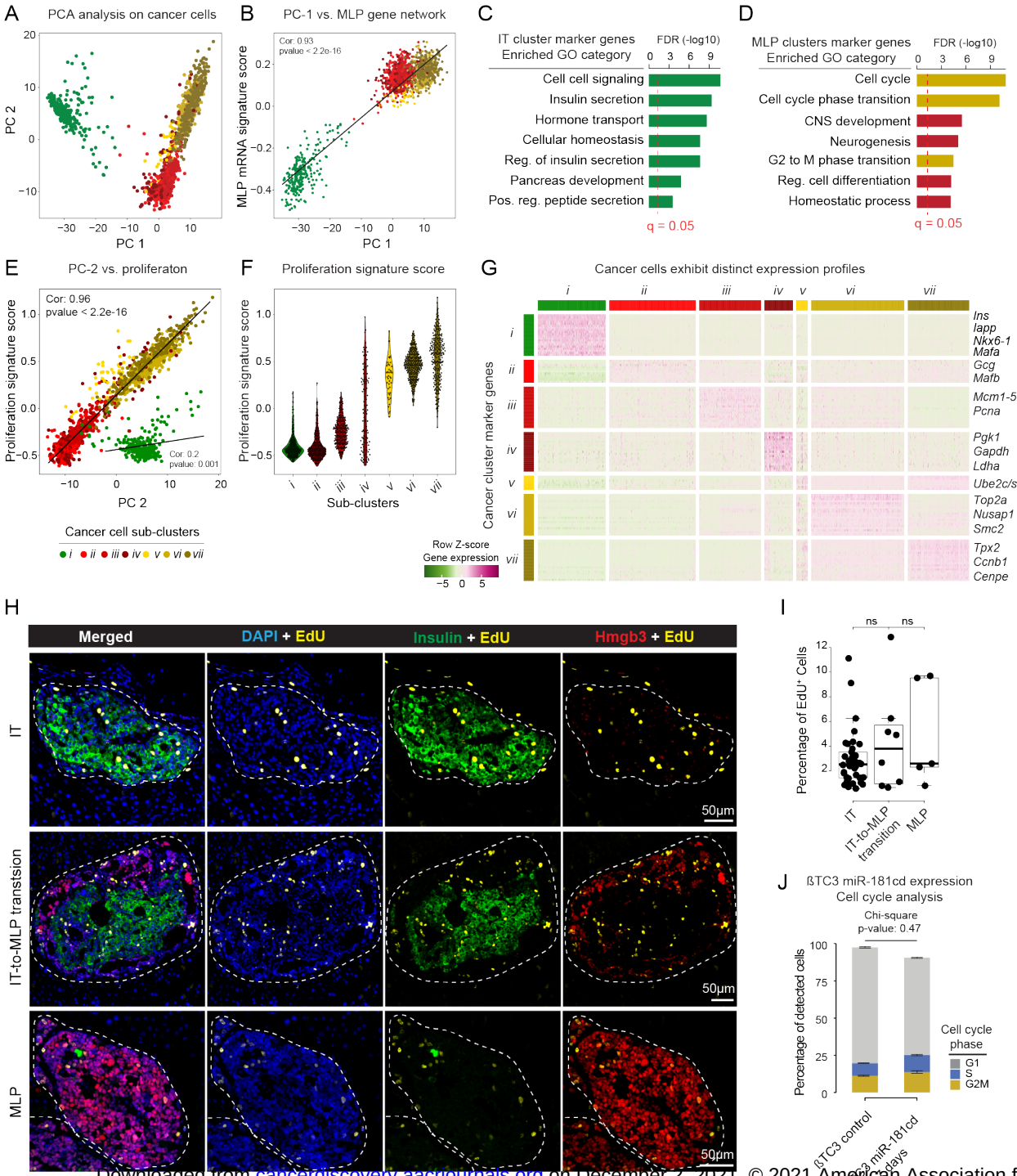

Figure 6

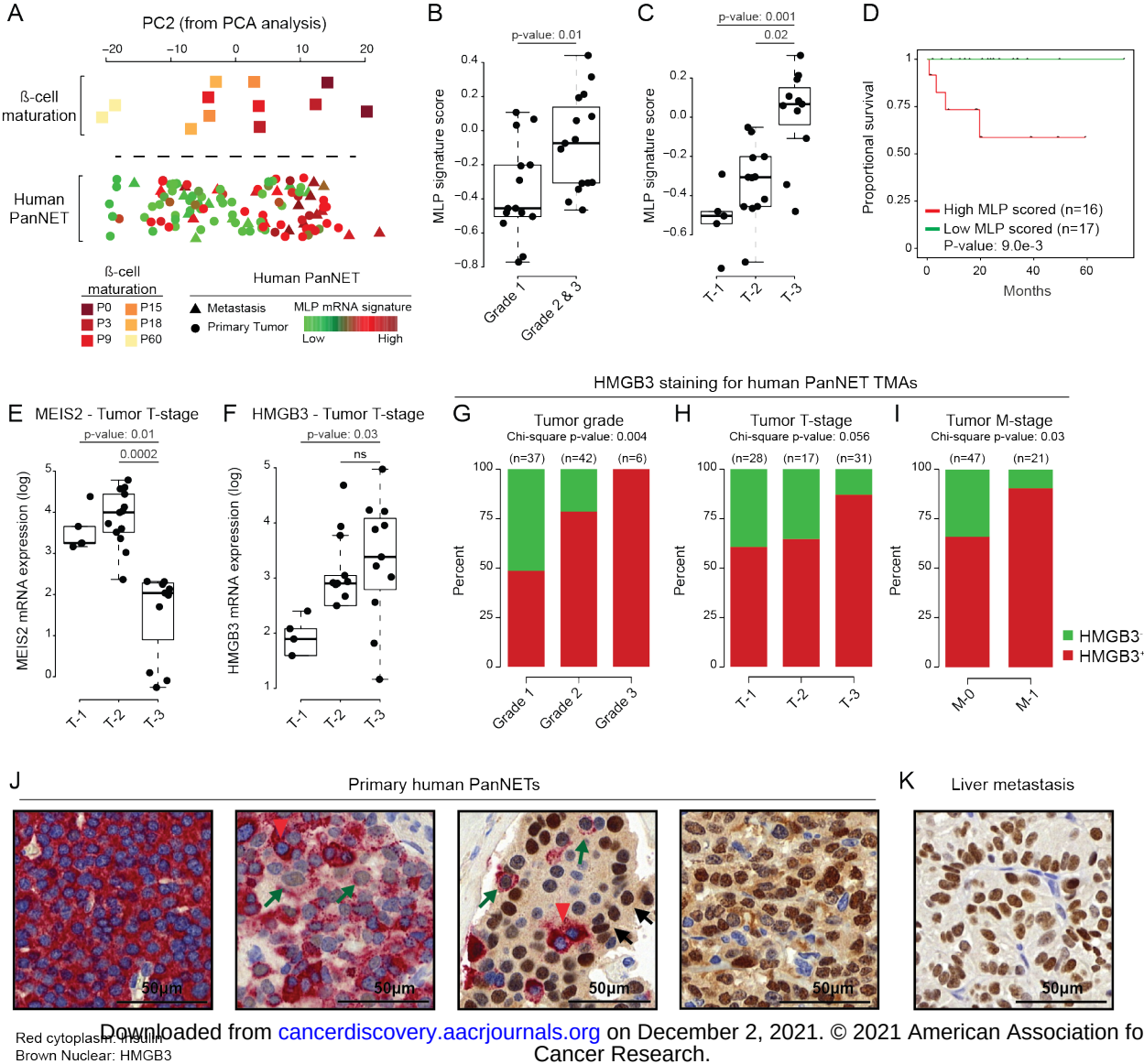

Red cytoplasm: Insulin
Brown Nuclear: HMGB3

AACR American Association for Cancer Research

CANCER DISCOVERY

Cancer cells retrace a stepwise differentiation program during malignant progression

Sadegh Saghafinia, Krisztian Homicsko, Annunziata Di Domenico, et al.

Cancer Discov Published OnlineFirst April 28, 2021.